Forest Ecology and Management 541 (2023) 121056

Contents lists available at ScienceDirect

Forest Ecology and Management

journal homepage: www.elsevier.com/locate/foreco

Discerning Oriental from European beech by leaf spectroscopy: Operational and physiological implications

Petra D'Odorico [a,*], Meredith C. Schuman [b,c], Mirjam Kurz [d], Katalin Csilléry [e]

[a] Remote Sensing group, Swiss Federal Research Institute for Forest, Snow and Landscape research WSL, Zürcherstrasse 111, 8903 Birmensdorf, Switzerland
[b] Department of Geography, University of Zurich, Winterthurerstrasse 190, CH-8057 Zürich, Switzerland
[c] Department of Chemistry, University of Zurich, Winterthurerstrasse 190, CH-8057 Zürich, Switzerland
[d] Environmental Genomics and Systems Biology Research Group, Institute of Natural Resource Sciences, Zurich University of Applied Sciences ZHAW, Wädenswil, Switzerland
[e] Evolutionary genetics group, Swiss Federal Research Institute for Forest, Snow and Landscape research WSL, Zürcherstrasse 111, 8903 Birmensdorf, Switzerland

ARTICLE INFO

Keywords:
Assisted migration
Fagus sylvatica L.
Fagus sylvatica subsp. *Orientalis*
Hyperspectral data
Species classification
Leaf traits

ABSTRACT

European beech (*Fagus sylvatica* L.) forests have recently experienced severe diebacks that are expected to increase in future. Oriental beech (*Fagus sylvatica* spp. *orientalis (Lipsky) Greut. & Burd*) is a potential candidate for assisted migration (AM) in European forests due to its greater genetic diversity and potentially higher drought resistance. Yet AM entails not only benefits, but also risks, and it is therefore important to monitor the progression of introduced (sub)species. Here, we demonstrate the potential of leaf spectroscopy to replace resource-intensive genetic analysis and field phenotyping for the discrimination and characterization of these two beech subspecies.

We studied two European beech forests, one in France and one in Switzerland, where Oriental beech from the Greater Caucasus was introduced over 100 years ago. During two summers (2021, 2022), we measured leaf spectral reflectance, leaf morphological and biochemical traits from genotyped adult trees. Subspecies prediction models were developed separately for top-of-canopy leaves (amenable to remote sensing) and bottom-of-canopy leaves (easier to harvest) using partial least squares discriminant analysis (PLS-DA) and different sets of spectral predictors.

Morphological, biochemical and spectra-derived leaf traits indicated that Oriental beech trees at the sites studied were characterized by higher lignin and nitrogen per unit leaf area than European beech, suggesting more protein-rich leaves on a per-area basis. The model based on top-of-canopy leaf reflectance spectra in the short-wave-infrared region (SWIR I: 1450–1750 nm) most accurately distinguished Oriental from European beech ($BA = 0.86 \pm 0.08$, $k = 0.72 \pm 0.15$), closely followed by models based on SWIR II, and on spectra-derived traits ($BA \geq 0.84$, $k \geq 0.67$).

This study provides a proof-of-principle for the development of spectroscopy-based approaches when monitoring introduced species, subspecies or provenances. Our findings hold promise for upscaling to large forest areas using airborne remote sensing.

1. Introduction

Current rates of global change outpace the ability of species to adapt and decouple tree populations from the environments to which they are locally adapted (Aitken et al., 2008; Anderson and Wadgymar, 2020). While slow migration rates delay many taxa from populating newly suitable climatic regions (Corlett and Westcott, 2013), the increasing frequency and duration of extreme climatic events challenge the limits of physiological tolerance for many species, whose morphological and biochemical acclimation mechanisms are no longer sufficient (Anderegg et al., 2019). These trends may push populations of major temperate tree species beyond their physiological recovery margins and could lead to massive die-off events (Forzieri et al., 2021; Neumann et al., 2017; Senf et al., 2018; Stanke et al., 2021).

Among the species which appear to suffer from global change in their current range is European beech (*Fagus sylvatica* L.) (Martinez del

* Corresponding author.
E-mail address: petra.dodorico@wsl.ch (P. D'Odorico).

https://doi.org/10.1016/j.foreco.2023.121056
Received 20 February 2023; Received in revised form 19 April 2023; Accepted 21 April 2023
Available online 8 May 2023
0378-1127/© 2023 The Author(s). Published by Elsevier B.V. This is an open access article under the CC BY license (http://creativecommons.org/licenses/by/4.0/).

Castillo et al., 2022): a widespread, ecologically and economically important species in Europe (Geßler et al., 2007). The distribution of European beech is limited in its southern and southeastern extent by drought (Jump et al., 2006; Peñuelas et al., 2008), but damage and die-off events associated with direct and indirect impacts of droughts have been recorded in the center of the species range as well (Obladen et al., 2021). In 2018, a severe, hot summer drought resulted in widespread premature leaf senescence in large parts of Germany and Switzerland, with continuously increasing cumulative tree mortality recorded in the following years (Frei et al., 2022; Klesse et al., 2022). Martinez del Castillo and colleagues (2022) suggested that the Europe-wide pervasive beech growth rate declines observed in the past decades will increase in the future, with 20% to over 50% less growth by 2090 depending on the climate change scenario and the region; and that only sites located towards the northern edge of the species range in Denmark, Norway and Sweden, and at higher elevation in mountain regions, will be able to maintain or increase current growth rates.

Oriental beech (*Fagus sylvatica* subsp. *Orientalis (Lipsky) Greut. & Burd*) is a subspecies of European beech, growing in the southeastern Balkans (Bulgaria and Greece), in the Pontic and Taurus Mountains (Turkey), in the Greater Caucasus (Georgia and Armenia) and in the Elbruz Mountains (Iran) (Kandemir and Kaya, 2009). Oriental beech is older than European beech and harbors high levels of genetic diversity across its range (Cardoni et al., 2022; Kurz et al., 2023). Oriental beech further inhabits some sites which are warmer and drier than those inhabited by European beech, and thus it is thought that some provenances might better acclimate to future climatic conditions in Europe (Bogunović et al., 2020; Fang and Lechowicz, 2006; Mellert and Seho, 2022).

Assisted migration (AM) is the human-aided translocation of individuals to mitigate the adverse effects of climate change by increasing forest diversity and thus resilience (Aitken and Whitlock, 2013; McLachlan et al., 2007). While such dynamic conservation measures entail ecological risks related to invasiveness of exotic species or outbreaks of new diseases (Winder et al., 2011), introducing close relatives of native species or populations from different parts of the species range, so-called assisted gene flow (AGF) (or, in a forestry setting, predictive provenancing; Hällfors et al., 2014), can be an efficient tool to introduce adaptive genetic variants, in an attempt to preserve a species rather than replace it with a new one (Aitken and Bemmels, 2016). However, AGF may also imply risks that could become apparent only in later generations, due to outbreeding depression (Grummer et al.; 2022), calling for monitoring. Yet, the similar appearance of introduced genotypes, and their hybridization, with the native provenances or subspecies, poses a challenge. Differences in leaf morphology, e.g., leaf size, shape and number of veins, between individuals of European and Oriental beech have been reported (Denk et al., 2002); however, these differences are not sufficient to distinguish the two with confidence, especially in the presence of hybrids. Genetic screening, therefore, currently represents the only reliable tool for accurate subspecies discrimination (Kurz et al., 2023). This is associated with high costs and multi-step extraction and analysis procedures, limiting our ability to monitor large geographic areas.

Reflectance spectroscopy, i.e., capturing the profile of light scattered back from leaves and canopies across a range of wavelengths, has emerged as an important tool for characterizing plant phyla and functional groups (Cavender-Bares et al., 2022; Meireles et al., 2020). Because the chemistry and structure of plant tissues govern their optical properties, plant reflectance spectra represent integrated measures of plant phenotypes, allowing for classification of taxa (Kothari and Schweiger, 2022). Yet, the use of reflectance spectroscopy to capture taxonomic patterns is not trivial, as environmental filtering effects and biotic interactions modulate the connection between species (and genotypes) and phenotypes in complex ways (Asner and Martin, 2011; Durán et al., 2019; Meireles et al., 2020; Siefert et al., 2015). High-dimensional spectral data has been used to classify genotype groups and species across climate zones and ecosystems at various levels of biological organization (Castro-Esau et al., 2006; Clark et al., 2005; Czyż et al., 2020; Madritch et al., 2014; Meireles et al., 2020), for monitoring invasive species (Asner et al., 2008), and for the development of biodiversity indicators (Schweiger et al., 2018). Spectral discrimination capacity, however, decreases with decreasing hierarchical levels of biological organization and with increasing trait similarity, as is expected among more closely related taxa (Cavender-Bares et al., 2016; Petibon et al., 2021).

Here, we examine the potential of leaf reflectance spectroscopy to distinguish European from Oriental beech at two European beech forests in France and Switzerland, where Oriental beech from the Caucasus was introduced>100 years ago. We conducted our investigation across two growing seasons in one site, and across two sites in one growing season, to account for year- and site-specific effects. We aimed to evaluate whether leaf spectra allow subspecies discrimination and, more specifically, (1) understand the physiological mechanisms behind a successful - or unsuccessful – subspecies separation by investigating spectra-derived and laboratory measured leaf functional traits; (2) understand whether leaves at the top of the canopy (more amenable to remote sensing in view of a potential upscaling) and at the bottom of canopy (easier to sample) hold equal discrimination potential, and (3) identify parts of the spectrum that best discriminate subspecies, including the full electromagnetic spectrum, individual spectral regions, and individual bands combined as functional trait indices.

2. Materials and methods

2.1. Study sites

This study was set at two, 100-year-old beech forest stands where Oriental beech was planted next to European beech. The first stand was located close to the town of Allenwiller (48°39′00.0′'N, 7°21′00.0′'E, 314 m a.s.l.) in northern Alsace, France. Oriental beech of the Greater Caucasus origin was planted there in 1923 (Klein, 1981; Kurz et al., 2023). At the time of our study, approximately 60 adult Oriental beech trees were identified in a 0.5 ha forest patch surrounded by a European beech forest except for a spruce plantation on its north side. The total size of the beech stand is 4.5 ha with trees reaching up to 40 m in height and having a mean DBH of 41 cm. The second forest stand is located close to the town of Wäldi (47°37′46.0″N, 9°06′17.4″E, 610 m a.s.l.) in the canton of Thurgau, in Switzerland (Kurz et al. 2023). An unknown number of Greater Caucasus-origin Oriental beech trees were planted there in 1921, but at the time of our study, only eight mature adult trees were present according to the cantonal forest service (Ulrich Ulmer, personal communication). Nevertheless, during the genotyping, we discovered six smaller but adult (DBH > 19 cm) Oriental beech trees. The size of the beech stand was approximately 3.3 ha, surrounded by a European beech forest to the south, and by agricultural land on all other sides, with trees reaching 40 m in height and having a mean DBH of 48 cm.

2.2. Selection of target trees

We selected a total of 94 adult trees for leaf reflectance spectroscopy measurements and functional trait determination at the two forest stands. Tree positions were recorded using a GPS (Trimble Geoexplorer 6000 series GeoXH) and imagery was acquired with a multispectral camera (Micasense RedEdge-MX DUAL) onboard an off-the-shelf unoccupied aerial vehicle (UAV; DJI Matrice 210, DJI Technology Co., Ltd., Shenzhen, China) and used to generate true-color orthomosaics of the study areas (Fig. 1 a,b).

Sampling was performed in Allenwiller in 2021 and 2022 (Table S1). We preferentially sampled trees for which the tops of canopies were easily accessible, which resulted in a bias towards larger Oriental beech individuals. In 2022, we adjusted our sampling to correct for this bias

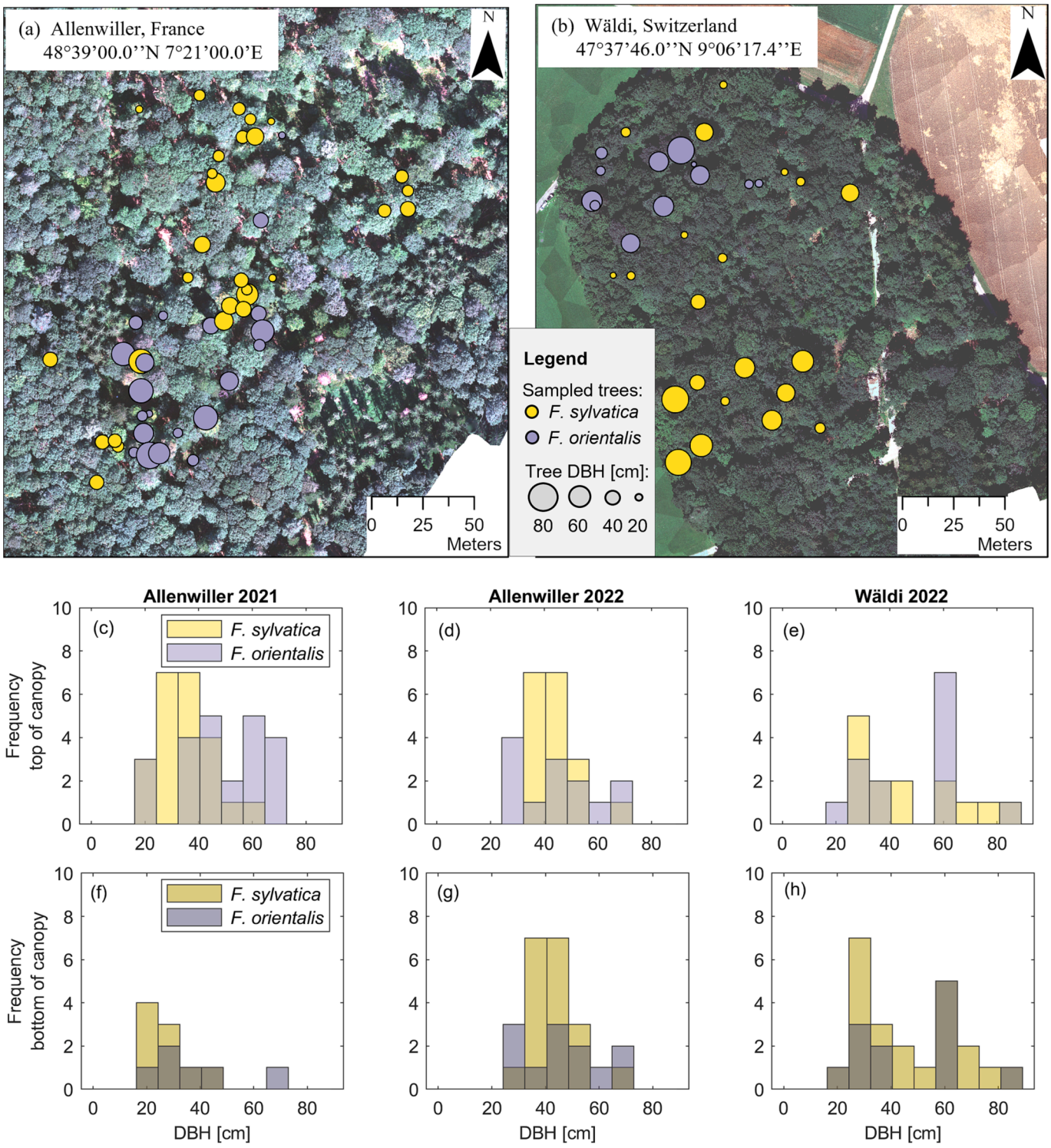

Fig. 1. Distribution (a, b) and diameter at breast height (DBH; c-h) of European (*F. sylvatica*) and Oriental (*F. orientalis*) beech trees sampled at the top and bottom of the canopy for leaf reflectance spectroscopy measurements and functional traits determination in Allenwiller, France (summer 2021 and 2022) and Wäldi, Switzerland (summer 2022). Orthomosaics (a, b) were generated from imagery acquired with multispectral sensor onboard an unoccupied aerial vehicle (UAV). In Wäldi (b) two of the mature Oriental beech trees are located about 100 m away in a forest patch not covered by the orthomosaic.

and sampled other Oriental and European beech individuals of similar size (Fig. 1, Table S1). In 2021, we collected 23 samples of both European and Oriental beech trees on 17–19 July, 31 of August and 1–2 September 2021 (only 6 and 9 samples for bottom leaves, Table S1), while, in 2022, we sampled 19 and 13 individuals of European and Oriental beech, on 19–22 July 2022. Overall, 9 individuals were sampled in both years. In Wäldi, we collected samples of 24 European and 14 Oriental beech individuals during 11–13, 18 and 25 of July 2022 (only 14 samples for European beech top canopy, Table S1).

2.3. Microsatellite genotyping

To confirm the taxonomic identity of the sampled trees, we genotyped leaf samples using 16 microsatellite loci (Lefèvre et al., 2012). Kurz and colleagues (2023) showed that these loci were sufficient to distinguish the two subspecies and their F1 hybrids unambiguously. DNA isolation and microsatellite genotyping were performed according to Kurz et al. (2023). Of the selected adult trees, 9 of those in Wäldi and 15 of those in Allenwiller were previously genotyped (Kurz et al., 2023). Thus, in Wäldi, 29 additional trees and in Allenwiller, 41 additional trees were genotyped for this study.

2.4. Field spectroscopy measurements

Leaves were sampled from the sunlit top third of the canopy as well as from the predominantly shaded bottom third to allow for large differences in canopy leaf traits associated with light exposure (Bachofen et al., 2020). Twigs at the bottom of the canopy were sampled using a handheld extendable pruner and twigs at the canopy top were mostly sampled using the DeLeaves twig sampling tool (DeLeaves, Sherbrooke, Canada, Charron et al., 2020), operated from a UAV (DJI Matrice 600, DJI Technology Co., Ltd., Shenzhen, China). The DeLeaves sampling tool comprises a carbon-fiber rod on which a grasping mechanism, a rotating saw, a branch-holding mechanism and a camera are installed (for details, see Charron et al., 2020). In a few cases, when trees were subdominant, the pruner was used for top-of-canopy sampling, because of difficulty in accessing these canopies using the drone-mounted system. Trees were sampled by climbing when the pruner or DeLeaves sampling device could not be employed. The sampling time window spanned from ca. 09:30 am to ca. 05:30 pm on prevalently sunny days and targeted one twig of ca. 0.5–1 cm diameter per canopy position and tree. The sampled twigs were immediately placed in water buckets and measured for leaf spectroscopy within half an hour of cutting.

Leaf spectroscopy reflectance measurements were performed using a portable spectroradiometer (FieldSpec 4 S/N 18739, ASD Inc., Boulder, CO, USA) coupled with a plant probe plus leaf clip extension. The FieldSpec spectroradiometer included three detectors covering the visible and near infrared (VNIR) to the shortwave infrared (SWIR) range, from 350 to 2500 nm (ASD, 2015). The plant probe was equipped with an internal standardized halogen light source allowing the measurement to be taken independently of external illumination. Measurement uncertainties associated with a similar set-up have been found to vary between 0.2 and 3% of the mean leaf reflectance in the VNIR and averaging 0.08% in the SWIR, according to Petibon and colleagues (2021), who reported that these uncertainties are small compared to the biological variation in leaf reflectance within and between individuals of European beech. Petibon and colleagues (2021) used a more complex protocol, measuring every leaf in front of both black and white standard leaf clip backgrounds and calculating reflectance from these measurements combined with measurements of the bare backgrounds, based on a simple model of leaf optical properties (5 spectra per condition). Because we were interested in relative differences between subspecies, we measured leaves only in front of the standardized black background of the leaf clip, thus measuring predominantly light scattered back from the leaf surface, and not back-scattered from a white background after initial penetration of the leaf. For this, three fully expanded healthy green leaves, taken from three different ramifications of the same twig, were selected for measurement. Leaf spectra were acquired from the adaxial leaf surface, at or close to the mid-point between the main vein and the leaf edge, and approximately half-way from petiole to leaf tip. One measurement was performed per leaf after waiting a few seconds for the spectrum, displayed live by the ASD software, to stabilize.

2.5. Field and laboratory measurements of leaf traits

For independent trait determination based on traditional field and lab protocols, we selected four traits known for their strong linkage with overall plant functioning, namely leaf thickness (LT), leaf mass per area (LMA), leaf carbon (C) and nitrogen (N) content (Hikosaka, 2004; Poorter et al., 2009; Wright et al., 2004). This set of measured traits was meant to complement and validate specifically for beech spectra-derived traits known to be more difficult to estimate from reflectance spectra due to overlap or absence of specific absorption features.

Leaf thickness was measured in the field on the same three leaves selected for spectroscopy. Measurements were performed at three interveinal regions at the middle of the leaf and on one side of the midvein, using a digital micrometer and a dial test indicator with a low measuring force of $\leq$ 0.15 N to allow consistent thickness measurements, e.g., not affected by leaf hairs or trichomes (Helios Preisser, model 0715, accuracy 0.002 mm). A brass cylinder was affixed to the ball tip of the dial test indicator with the flat surface flush against the micrometer, to ensure uniform and gentle pressure and avoid compressing the leaf at the ball point. Contact pressure was further minimized by approaching the point of zero displacement of the dial indicator. Leaves were next wrapped in tinfoil and stored on ice in coolers for transport within a few days to the laboratory, for further processing.

To determine LMA, 0.12 cm^2 discs were punched from three middle interveinal regions on each leaf, oven dried at 60 °C for 48 h and weighed using a precision balance to determine dry weight. A slightly different protocol was used during the August 2021 Allenwiller campaign, when fresh leaf area was determined using leaf scanned images and analyzed with the open-source ImageJ software (Abràmoff et al., 2004). The leaf disc protocol was chosen for subsequent campaigns due to the higher efficiency and reproducibility, and better correspondence with leaf spectroscopy measurements. Oven-dried samples were next ground and homogenized using a ball mill (Retsch M200, Haan, Germany) and subsequently analyzed using an elemental analyzer (Flash EA, Thermo Italy, Rhodano, Italy) to obtain nitrogen and carbon concentrations per unit mass. The equivalent nitrogen (N_A) and carbon (C_A) content per unit leaf area were calculated using the LMA, to be in line with their estimation based on leaf spectra using a fixed-area leaf clip.

2.6. Statistical analysis

2.6.1. Subspecies classification from genetic data

Kurz and colleagues (2023) identified five genetic clusters of Oriental beech corresponding to five distinct mountain ranges within its distribution. Following Kurz and colleagues (2023), we used the Bayesian clustering method implemented in the software Structure version 2.3.4 (Pritchard et al., 2000) to estimate the taxonomic identity of the newly genotyped trees and to test if they also originate from the Greater Caucasus. We used the model with correlated allele frequencies and admixture and considering models from one to seven clusters (K values). We eliminated the first 1,000,000 iterations as a burn-in period, and we used the following 500,000 iterations for estimation. Kurz and colleagues (2023) found that the assignment of new individuals to previously identified clusters using the USEPOPINFO model of Structure performed less well than applying the clustering algorithm to a full data set composed of a reference data set (i.e., samples from the natural range) and individuals of unknown origin. Therefore, we did not use the USEPOPINFO model for assignment. We ran ten independent chains for each K and averaged them using CLUMPAK (Kopelman et al., 2015). We also used STRUCTURE HARVESTER version 0.6.94 (Earl and vonHoldt, 2012) to estimate the number of clusters that best explained our data, considering the log likelihood of each K (L(K) method; Pritchard et al., 2000) and the ad hoc statistic ΔK (Evanno method; Evanno et al., 2005).

2.6.2. Leaf reflectance spectra and spectra-derived traits

All reflectance spectra were trimmed to 400–2400 nm by removing ends characterized by high noise and corrected for radiometric steps

occurring at the transition regions between detectors due to temperature changes (Hueni and Bialek, 2017). Spectra measured in close sequence on three leaves of the same twig were next averaged to obtain one mean spectrum per individual tree, campaign, and canopy position. In the initial screening, data from sites and years were pooled together to increase the sample size, but top- and bottom-canopy leaves were analyzed separately. Intraspecific variation in leaf reflectance for each tree and subspecies was quantified through the coefficient of variation (CV), calculated as the standard deviation divided by the mean over all individuals' spectra. Interspecific variation was instead quantified using the spectral separability index (SSI), indicating the importance of each wavelength in distinguishing between the two subspecies and calculated as:

$$SSI = \frac{\left|\mu_{\lambda Orientalis} - \mu_{\lambda Sylvatica}\right|}{s_{\lambda Orientalis} + s_{\lambda Sylvatica}} \quad (1)$$

where $\mu_{\lambda class}$ is the mean reflectance value at a given wavelength and $s_{\lambda class}$ is the standard deviation of the wavelength within the given leaf class, i.e., *sylvatica* or *orientalis* (Asner et al., 2018).

Spectra-derived traits were obtained based on existing indices obtained from the literature (see Table 1). Indices were obtained by combining reflectance at wavelengths sensitive to the presence and concentration of a specific leaf constituent, i.e., showing an absorption feature, and a constituent-independent reference wavelength. For N and LMA, linear regression and Pearson correlation coefficients were computed for spectra-derived traits versus laboratory measurements. Next, we conducted a Principal Component Analysis (PCA) on the scaled spectra-derived trait data to determine whether leaf traits co-vary in a coordinated manner and how subspecies arranged within the trait space.

Table 1
Spectral indices used for the estimation of spectra-derived traits.

Spectra-derived trait	Spectral index	Reference
Leaf mass per area (sLMA)	Normalized difference index for LMA: $ND_{LMA} = \frac{R_{1368} - R_{1722}}{R_{1368} + R_{1722}}$	Féret et al., 2011
Nitrogen (sN)	Normalized Difference Nitrogen Index: $NDNI = \frac{log\left(\frac{1}{R_{1510}}\right) - log\left(\frac{1}{R_{1680}}\right)}{log\left(\frac{1}{R_{1510}}\right) + log\left(\frac{1}{R_{1680}}\right)}$	Fourty et al., 1996; Serrano et al., 2002
Cellulose (sCell)	Cellulose Absorption Index: $CAI = 0.5(R_{2000} + R_{2200}) - R_{2100}$	Daughtry et al., 2004
Lignin (sLig)	Normalized Difference Lignin Index: $NDLI = \frac{log\left(\frac{1}{R_{1754}}\right) - log\left(\frac{1}{R_{1680}}\right)}{log\left(\frac{1}{R_{1754}}\right) + log\left(\frac{1}{R_{1680}}\right)}$	Fourty et al., 1996; Serrano et al., 2002
Chlorophyll (sChl)	Leaf Chlorophyll Index: $LCI = \frac{R_{850} - R_{710}}{R_{850} + R_{680}}$	Datt, 1999; le Maire et al., 2004
Chlorophyll Carotenoids ratio (sChlCar)	Chlorophyll/Carotenoid index: $CCI = \frac{R_{528} - R_{645}}{R_{528} + R_{645}}$	Gamon et al., 2016
Anthocyanin (sAnth)	Anthocyanin Reflectance Index: $ARI2 = R_{800} * \left(\frac{1}{R_{550}} - \frac{1}{R_{700}}\right)$	Gitelson et al., 2001
Water (sWater)	Normalized Difference Water Index: $NDWI = \frac{R_{857} - R_{1241}}{R_{857} + R_{1241}}$	Gao, 1996
Wax (sWax)	Leaf Wax index: $EWI = R_{625} * \left(\frac{1}{R_{736}} - \frac{1}{R_{832}}\right)$	Camarillo-Castillo et al., 2021

2.6.3. Trait variation within and between subspecies

To examine the variance explained by site, year, canopy position, DBH and subspecies on individual leaf traits (i.e., either derived from spectra or through field and lab protocols), we used linear mixed-effect models (LMM) on pooled data with site, year, canopy position, DBH and subspecies as fixed effects, and with tree ID included as a random effect to account for pseudo-replication on the tree level, as a few trees were sampled twice, once in July and once in August (different twigs). Next, to examine subspecies differences more closely in leaf traits and to investigate whether they persist across canopy positions, sites, and years, we used LMM on individual canopy position / site / year data subsets. Subspecies was considered a fixed effect and tree 10 cm DBH class was incorporated as a random effect influencing the model intercept. For the dataset collected in Allenwiller in 2021, tree ID was further included as a random effect to account for replicate measure at the tree level. The restricted maximum likelihood (REML) method was used to fit LMMs and obtain estimates and significances of effects using Matlab (version 9.5.0 R2018b). REML is known to be more robust in accommodating unbalanced designs characterized by an unequal number of observations, as is common in ecological studies (Spilke et al., 2005). Homoscedasticity and normality of residuals were verified visually. The significance and the effect size of subspecies on traits were evaluated based on p-values and Cohen's d value, calculated as the difference between group means divided by the pooled standard deviation (Sullivan and Feinn, 2012).

2.6.4. Subspecies classification from spectral data

We used partial least square discriminant analysis (PLS-DA) to test the potential of leaf reflectance spectra to discriminate individuals of Oriental and European beech. PLS-DA is suitable for overdetermined datasets where the number of independent variables is larger than the sample size because it transforms a set of correlated explanatory variables into a new set of uncorrelated variables (Chevallier et al., 2006; Wold et al., 2001). PLS-DA still requires a large sample size to improve prediction performance. We thus used pooled data across sites and years, which also allowed us to test whether the two subspecies can be discriminated irrespective of the variation across sites and years. We assessed the utility of different sets of predictor variables for discriminating between the two subspecies, subsequently referred to as models. A total of twelve models differing by canopy position from which measured leaves originated, i.e., top or bottom, and by set of predictors, were evaluated. Predictor sets included reflectance at wavelengths encompassing: (i) the full spectrum (400–2400 nm), (ii) the visible (VIS: 400–750 nm), (iii) the near-infrared (NIR: 750–1300 nm), (iv) the short-wave-infrared I (SWIR I: 1450–1750 nm), or (v) the short-wave-infrared II (SWIR II: 1950–2400 nm) spectrum, and (vi) nine spectra-derived traits. Logarithmic transformation and autoscaling (i.e., centering and variance scaling) was applied on the spectra-derived traits data to reduce skewness and obtain a comparable measurement scale (Ballabio and Consonni, 2013). A preliminary screening of the discriminatory power of spectra-derived trait predictors was performed using Wilks' lambda, ranging between 0 and 1, with lower values indicating a higher capability of the predictor variable to separate the considered classes. Since Wilks' lambda values represents univariate predictor indicators, all spectra-derived traits were still kept in the final model to explore the combined discrimination power.

PLS-DA was performed using Matlab (version 9.5.0 R2018b) routines modified from Ballabio and Consonni (2013). For each data set, we ran 100 iterations in which we randomly split the data into 50% calibration and 50% validation sets (new split each time) using identical subspecies class proportions and making sure the same individual never appeared in both calibration and validation sets. Model calibration was performed on the calibration set and included the selection of optimal number of latent variables (LVs) based on a 5-fold venetian blinds cross-validation procedure. The optimal number of LVs was selected as the number minimizing both the error rate and the number of unassigned samples.

Model learning and predictive ability were evaluated based on the area under the curve (AUC) of the receiver operating characteristics (ROC) curve for calibration and validation sets, respectively, averaged over 100 iterations. For the optimal threshold values, which minimize the risk associated with omission (sensitivity) and commission (1-specificity) errors during class assignment, we computed confusion matrices, from which balanced accuracy (BA) and Cohen's kappa coefficient (k) performance metrics were derived and averaged over the 100 iterations. Although BA is commonly used, it can be misleading as it only considers positive instances, while k represents a more robust metric also for unbalanced datasets, producing a high score only if the prediction is good in all four confusion matrix categories (Cohen, 1960). The number of samples not assigned (na) to any of the classes was further considered to evaluate classification performance.

3. Results

3.1. Subspecies classification from genetic data

In agreement with Kurz and colleagues (2023), we found that the best supported number of clusters was six, with five distinct Oriental beech clusters (Fig. S1). Further, we could assign all newly genotyped Oriental beech trees to the Greater Caucasian cluster (Fig. 2). The genetic clustering analysis thus confirmed that we sampled 31 European and 25 Oriental beech trees in Allenwiller, and 24 European and 14 Oriental beech trees in Wäldi.

3.2. Leaf reflectance spectra and spectra-derived traits

Intra- and interspecific subspecies variation in leaf reflectance differed by wavelength at the top (N = 105; Fig. 3a) and at the bottom (N = 84; Fig. 3b) of the canopy. Variation within a subspecies was greatest (CV > 20%) for top-of-canopy leaves in the visible region (VIS: 400–700 nm), while between-subspecies variation (SSI > 30%) was observed in the VIS near 518 nm and 680 nm (Fig. 3c). The greatest variation between subspecies (SSI_{top} = 29%, SSI_{bottom} = 20%) and lowest variation within subspecies (CV_{top} = 5%, CV_{bottom} = 6%) was found in the near-infrared region (NIR: 750–1300 nm), with Oriental beech trees characterized by higher reflectance in the NIR plateau. In the shortwave-infrared region (SWIR: 1300–2400 nm), relative variation between versus within subspecies strongly varied by wavelength and was driven by absorption features. The two water absorption features, centered at 1450 nm and 1850 nm, explained > 10% of variation observed within and between subspecies at the top of the canopy (Fig. 3c). Large variation (≥20%) between subspecies was also observed at the top and bottom of the canopy between 1650 and 1750 nm (Fig. 3c, d). We also tested for within-tree spectral variation and found a similar pattern as for within-subspecies variation, with the VIS region and the two water absorption features characterized by the highest variation (Fig. S2).

In a PCA of the 9 spectra-derived traits, the first principal component (PC1) explained 48% (top of canopy; Fig. 4a) and 59% (bottom of canopy; Fig. 4b) of the overall variation. Variables related to leaf structure and nutrient content, such as spectra-derived leaf mass per area (sLMA), lignin (sLig), cellulose (sCell) and nitrogen in proteins (sN) (Table S2), had the highest loading on PC1 for both bottom- and top-of-canopy leaves. PC2 explained 21% (top of canopy; Fig. 4a) and 19% (bottom of canopy; Fig. 4b) of variance, and mainly represented indices for pigments and waxes. Thus, traits correlated with PC2 are closely related to photosynthesis and photoprotection of leaves during high irradiance. The two subspecies appeared separated along PC1 in the multidimensional trait space for leaves at the top of the canopy (Fig. 4a). Specifically, Oriental beech had thicker leaves with higher protein-N (higher PC1 scores), while European beech had lower PC1 scores. In contrast, subspecies separation was not evident along PC2 or for leaves at the bottom of the canopy.

For the two traits, N and LMA, determined using both, spectral indices and laboratory protocols, linear regression analysis revealed strong positive relationships (N: $r \geq 0.77$, $p < 0.001$; LMA: $r \geq 0.82$, $p < 0.001$; Fig S3).

3.3. Trait variation within and between subspecies

Linear mixed-effects model on the pooled data revealed significant effects ($p < 0.05$) of canopy position, site and year on nearly all traits (Table S3). Canopy position showed the strongest effect, confirming well-known morphological and biochemical trait gradients along the canopy (see also Figs. 5-6). Overall, the second most important effect on trait variance was year, followed by site, which was found to have significant but weaker effects as compared to canopy position and year. Subspecies had a significant effect on leaf N, lignin, cellulose and Chl estimated from spectra, and for N and LT measured in the laboratory or field. Overall, DBH class had little effect on trait variation (Table S3).

Linear mixed-effects models for individual sites, years and canopy positions showed that at the top of the canopy, spectra-derived leaf nitrogen (sN) and lignin (sLig) differed between subspecies ($p \leq 0.05$, $d \geq 0.77$; Table 2). N per unit leaf area measured in the laboratory, also differed between subspecies, yet was only marginally significant inWäldi ($p \leq 0.077$, $d \geq 0.72$; Table 2). For all sites and years, Oriental beech had higher sLig and sN (and N; Fig. 6a-c) as compared to European

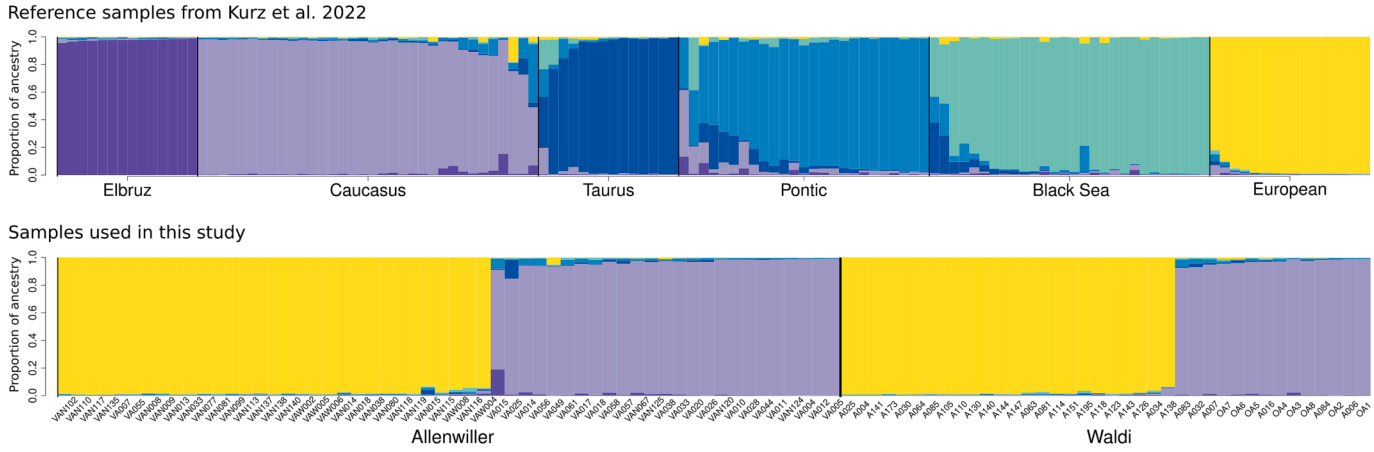

Fig. 2. Genetic characterization of the European and Oriental beech populations sampled in Allenwiller and Wäldi. Genetic clustering was performed using the software Structure assuming six clusters. Each bar corresponds to a sampled individual and each color to a genetic cluster that corresponds to the mountain ranges/regions considered in Kurz et al. 2023.

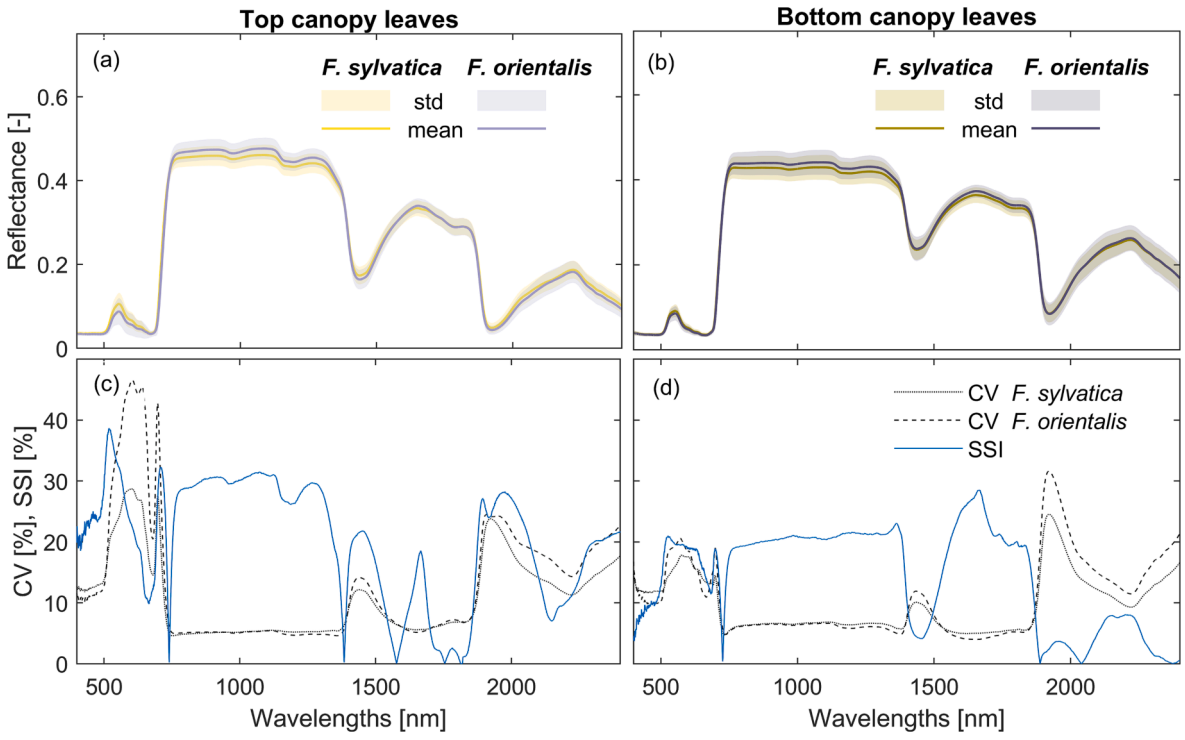

Fig. 3. Spectral variance within and between subspecies shown as original leaf reflectance spectra (a, b) and as coefficient of variation (CV) and spectral separability index (SSI, blue lines) (c, d). Results are shown for top *F. orientalis* (N = 50) and *F. sylvatica* (N = 55) and bottom *F. orientalis* (N = 32) and *F. sylvatica* (N = 52) canopy leaves measured for adult trees in Allenwiller, France (summer 2021 and 2022) and Wäldi, Switzerland (summer 2022). Leaf reflectance spectra were measured using a portable spectroradiometer acquiring in the visible (VIS: 400–750 nm), the near-infrared (NIR: 750–1300 nm), and the short-wave-infrared (SWIR: 1450–2400 nm).

beech (Fig. 5 a-f). For all other traits, significant subspecies effects were found for at most one or two (e.g., sChl, sChlCar, $p \leq 0.01$; Fig. 5 t,v,x) site-year instances. We note that traits linked with leaf structure, i.e., LMA and LT, for which we found significant subspecies effects in the first year of sampling (2021) in Allenwiller (Table 2, Fig. 5j, Fig. 6g,j), did not differ at either of the two sites in the following year (2022).

3.4. Subspecies classification from spectral data

For the trait-based model, a preliminary screening of the discrimination power of individual trait predictors using Wilks' lambda confirmed spectra-derived lignin (sLig) and nitrogen (sN), to have a relatively greater discrimination capacity for top-of-canopy leaves, indicated by Wilks' lambda values below 0.8 (Fig. S4).

Leaf canopy position was highly determinant in classification performance, regardless of the set of spectral predictors used in the model. Models based on leaves from the top third of the canopy always outperformed models using leaves originating from the bottom third, with mean AUC indicating moderate to high (AUC_{top} = 0.75 – 0.93) versus low (AUC_{bottom} = 0.52 – 0.75) discriminatory capacity over all thresholds, respectively (Fig. 7). This was confirmed by mean statistics obtained from confusion matrices for optimal threshold values, with fair to substantial agreement between predicted and actual classes using top-of-canopy leaves (BA_{top} = 0.71–0.86; k_{top} = 0.40 – 0.72) and poorer agreement using bottom-of-canopy leaves ($BA_{bottom} \leq 0.68$; $k_{bottom} \leq 0.34$; Table 3). Samples that could not be assigned to any of the classes remained the same for European beech (na = 0 –3%) but decreased for Oriental beech when using leaves originating from the top of the canopy (na_{top} = 0 – 4%; na_{bottom} = 0–8%; Table 3). The same improvement of top- over bottom-of-canopy leaves was found for model learning performances based on the calibration sets (Fig. S5, Table S5).

The best separation between Oriental and European beech individuals was obtained based on leaves from the canopy top by the model using as predictors bands in the 1450 –1750 nm region of the spectrum (SWIR I). This model resulted in a high mean classification accuracy, as evidenced by $AUC_{top} = 0.93 \pm 0.03$ (Fig. 7d), $BA_{top} = 0.86 \pm 0.08$ and $k_{top} = 0.72 \pm 0.15$ (Table 3), obtained over the 100 model iterations. This model was followed by models using as predictors spectra-derived traits, bands in the SWIR II, and the full spectrum, resulting in good classification performances for top-of-canopy leaves. We found the model based on the VIS region (400–750 nm) to have the worst performance, with low ($AUC_{bottom} = 0.53 \pm 0.08$; Fig. 7h) to fair ($AUC_{top} = 0.75 \pm 0.06$; Fig. 7b) mean classification accuracy for bottom- and top-of-canopy leaves, respectively, according to ROC curve analysis. Similarly, confusion matrix statistics indicated poor ($k_{bottom} < 0.1$) to fair ($k_{top} = 0.40 \pm 0.13$) mean agreement between predicted and actual classes using the VIS region at the bottom and top of the canopy, respectively (Table 3). Surprisingly, as it was in disagreement with what the spectral separability analysis based on SSI and CV indices seemed to suggest (Fig. 3), the NIR model showed the second-worse mean classification performance using the validation set. Models' performances ranked similarly for both, their learning and their predictive abilities, evaluated respectively on the calibration (Fig. S5, Table S5) and on the validation datasets (Fig. 7, Table 3). Interestingly, the percentage of unclassified samples was the metric least affected by model type, e.g., we found 4% of the Oriental beech individuals could not be assigned to any class by either the overall best (SWIR I) and the overall worst (VIS) performing model.

4. Discussion

We present a proof-of-principle study discriminating European and Oriental beech using leaf spectroscopy, and discuss physiological implications related with the functioning of the two subspecies under the same environmental conditions at two 100-year-old forest stands, as well as operational implications related with the choice of sensor and related wavelengths required for discrimination. We also discuss the next lines of research in terms of beech subspecies trait variation and

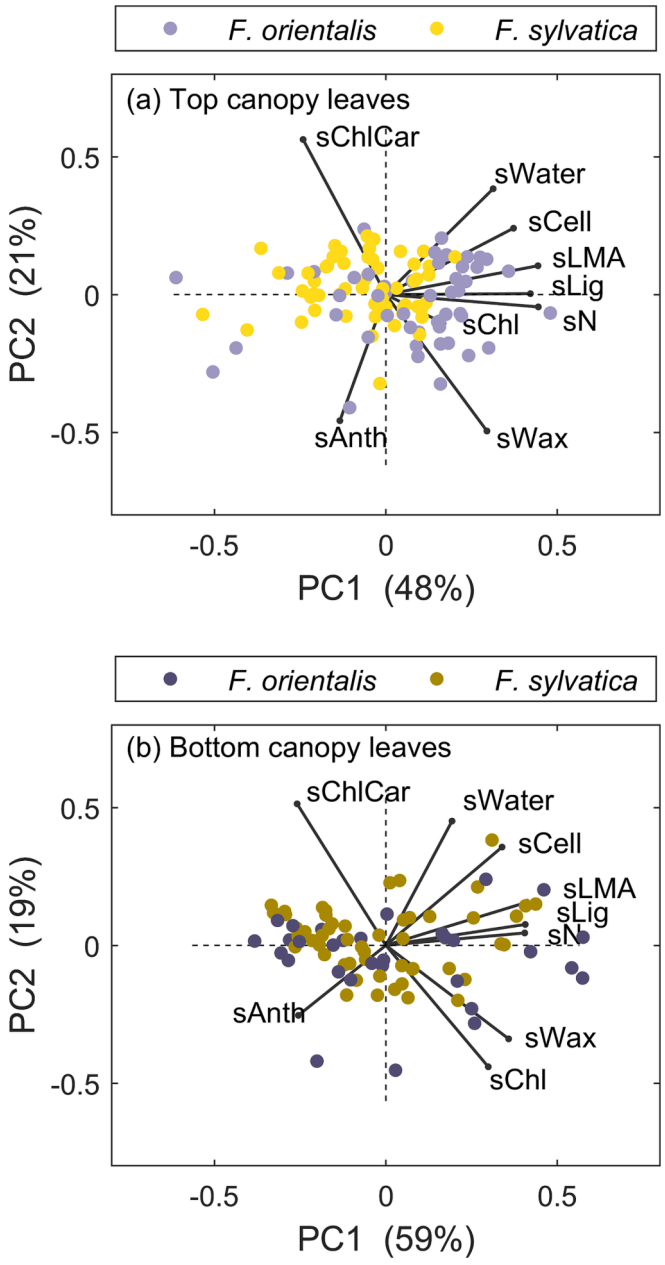

Fig. 4. Principal component analysis (PCA) of the 9 spectra-based leaf functional traits for top- (a; N = 105) and bottom- (b; N = 84) of-canopy leaves from *F. sylvatica* and *F. orientalis* in Allenwiller, France (summer 2021 and 2022) and Wäldi, Switzerland (summer 2022). Spectra-derived traits include: chlorophyll carotenoid pigment pools ratio (sChlCar), water content (sWater), cellulose (sCell), leaf mass per area (sLMA), lignin (sLig), nitrogen (sN), wax (sWax), chlorophyll pigments (sChl) and anthocyanin pigments (sAnth).

classification approaches in support of assisted gene flow.

4.1. Differences in leaf physiology of the two beech subspecies

At the leaf level, reflectance in the VIS is mainly driven by rapid pigment interconversion dynamics that occur in function of changing light conditions (D'Odorico et al., 2021). It follows that the high within-species spectral variance for top canopy leaves in the VIS (Fig. 3) is likely the result of sampling taking place over the course of an entire day and associated differences in leaves' light histories. The high between-subspecies spectral variance at the top of the canopy (SSI > 30%), observed near 518 nm and 680 nm (Fig. 3c), might instead result from subspecies differences in seasonal adjustments of carotenoid and chlorophyll pigment pools (Wong et al., 2019); a hypothesis that remains to be clarified using laboratory measures. In the NIR, variance between subspecies is likely associated with differences in leaf cell structure and light scattering within the leaf spongy mesophyll layer that determine leaf optical properties in this spectral region (Ollinger, 2011). Finally, in the SWIR, which we found to be the most informative region for discriminating Oriental and European beech, light-plant interactions at the leaf level are governed by non-pigment leaf constituents, including lignin, cellulose and N in proteins, influencing leaf optical properties directly through their individual absorption features, and indirectly via their relationship with structural and microstructural leaf traits such as cell wall composition and epidermis thickness (Ollinger, 2011; Poorter et al., 2009; Wright et al., 2004). Collectively, this suite of traits affecting SWIR reflectance reveals leaf construction investments supporting functions related to foliar longevity and defense, and controlling many physiological functions linked with photosynthetic capacity and stress avoidance (Kokaly et al., 2009; Kozhoridze et al., 2016; Wright et al., 2004). Strong absorption features of ligno-cellulose constituents of plant tissues and cell walls are found in the SWIR at 1680 nm and 1750 nm and from 2100 nm to 2300 nm (Curran, 1989; Serrano et al., 2002), and were used here to compute spectral indices for the estimation of these constituents (see Table 1). While these absorption features are affected by water content and overlay with other absorption features, cellulose and lignin are present in great abundance in leaves compared to other constituents which absorb in these regions (except for water) (Kokaly et al., 2009; Ollinger, 2011). Nitrogen, in contrast, is associated with more complex leaf optical properties (Kokaly, 2001). Low concentrations and partly overlapping absorption features of N-containing constituents with water and other dry matter constituents make its estimation from plant spectra challenging (Fourty et al., 1996; Féret et al., 2021). Nevertheless, our validation against laboratory determined leaf N ($r = 0.88$, $p \leq 0.001$; Fig. S3 a) suggests that it is feasible, consistent with several other studies (Ely et al., 2019; Kothari et al., 2023b,a; Serbin et al., 2014; Serrano et al., 2002). Nitrogen is present in leaves in many forms, which warrants caution in the formulation of physiological implications. Here, we estimated N using wavelengths in the SWIR (see NDNI in Table 1), linked with its presence in proteins (i.e., Ribulose-1,5-bisphosphate carboxylase/oxygenase, i.e., Rubisco), containing up to 50% of N of green leaves as compared to only 2% contained in Chl pigments (Hikosaka and Terashima, 1996). N allocated to cell walls may also have contributed, yet its concentration is reported to be relatively low (around 2.2%)(Onoda et al., 2004; Takashima et al., 2004). In addition to spectral indices, plant traits can be estimated from spectra also using other empirical and physical approaches. Among these, are physically-based radiative transfer models (Féret et al., 2021) and empirical models based on multivariate techniques such as partial least squares regression (PLSR) (see review by Kothari and Schweiger, 2022). These approaches are particularly interesting for traits that are characterized by overlapping or weak absorption features and that are lacking dedicated spectral indices.

This study represents a first step towards the spectral and functional characterization of two beech subspecies. Overall, our dataset suggests that in the two examined forest stands, Oriental beech trees are characterized by leaves with more lignin per unit leaf area and thus are likely tougher as compared to leaves from European beech trees growing under the same environmental conditions. While this was supported also by higher LMA and LT values for Oriental beech in 2021, this pattern was not apparent from the data collected in 2022, suggesting the effect of genotype × environment interactions. Indeed, the summers of 2021 and 2022 had drastically different meteorological conditions: 2021 was exceptionally wet and 2022 was exceptionally dry. Lower average air temperature (T_a) and irradiance (Rad), and higher relative humidity (RH) and precipitation (Precip), were recorded in both spring and summer of 2021 as compared to 2022 (Table S4). Preceding- and current-year conditions might have triggered greater environmental

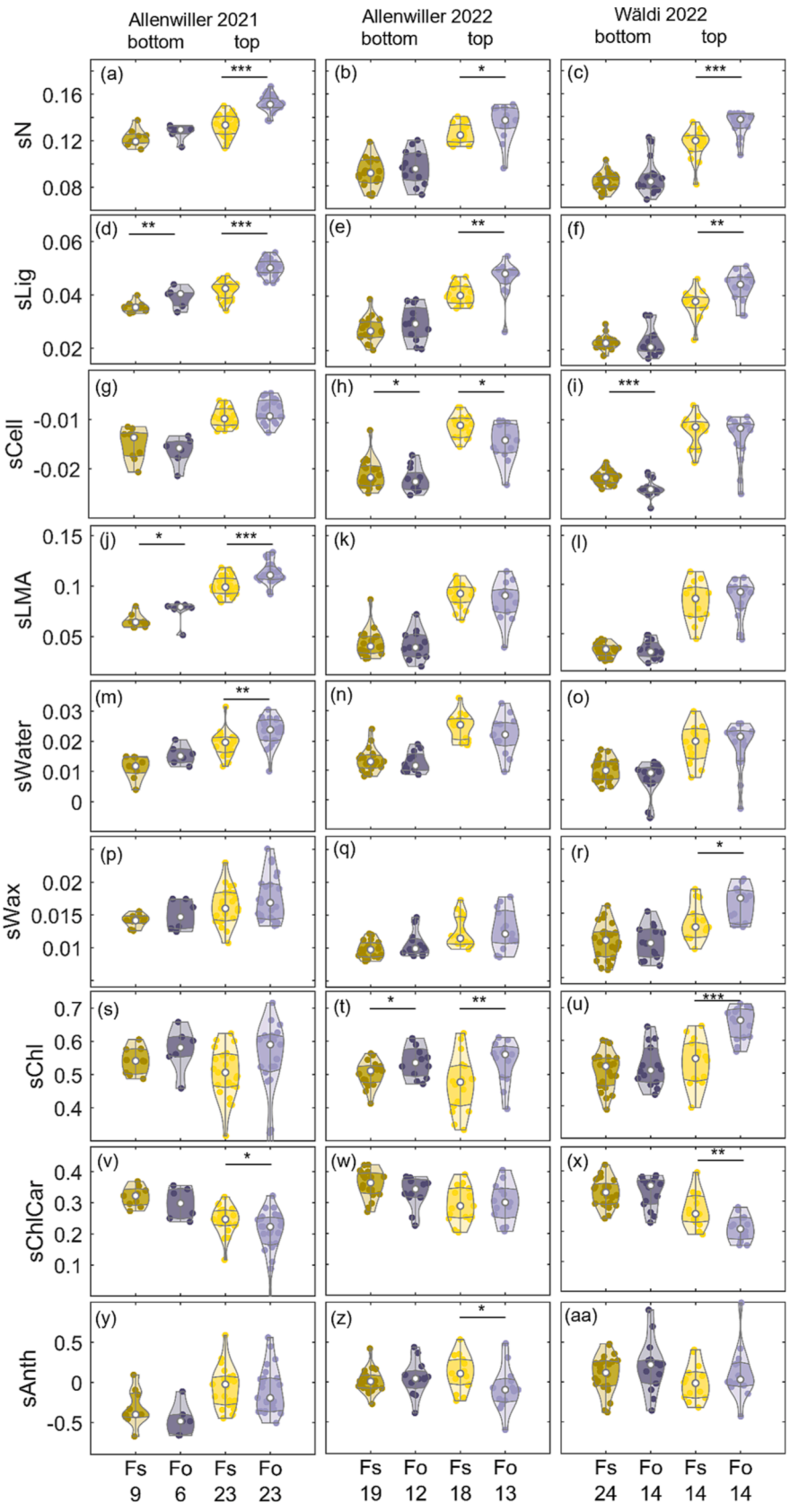

Fig. 5. Spectra-derived leaf traits of *F. sylvatica* (Fs) and *F. orientalis* (Fo) tree subspecies in Allenwiller, France (summer 2021 and 2022) and Wäldi, Switzerland (summer 2022). Violin plots show trait distributions, with circles representing median values and darker-colored areas representing intervals between the 25th and 75th quartiles. The number of samples for each subspecies (Fs, Fo) is indicated under the subspecies label. Asterisks above the violin plots indicate significant differences between subspecies at either bottom or top of canopy (* $p \leq 0.05$, ** $p \leq 0.01$, *** $p \leq 0.001$) according to linear mixed effect models, with subspecies as fixed effect and diameter at breast height class as random effect (for Allenwiller 2021, tree ID was additionally considered as random effect in the model). Spectral (s) indices used for estimation of leaf traits: nitrogen (sN; a-c), lignin (sLig; d-f), cellulose (sCell; g-i), leaf mass per area (sLMA; j-l), water content (sWater; m-o), wax (sWax; p-r), chlorophyll pigments (sChl; s-u), chlorophyll carotenoid pigment pools ratio (sChlCar; v-x), and anthocyanin pigments (sAnth; y-aa), are reported in Table 1.

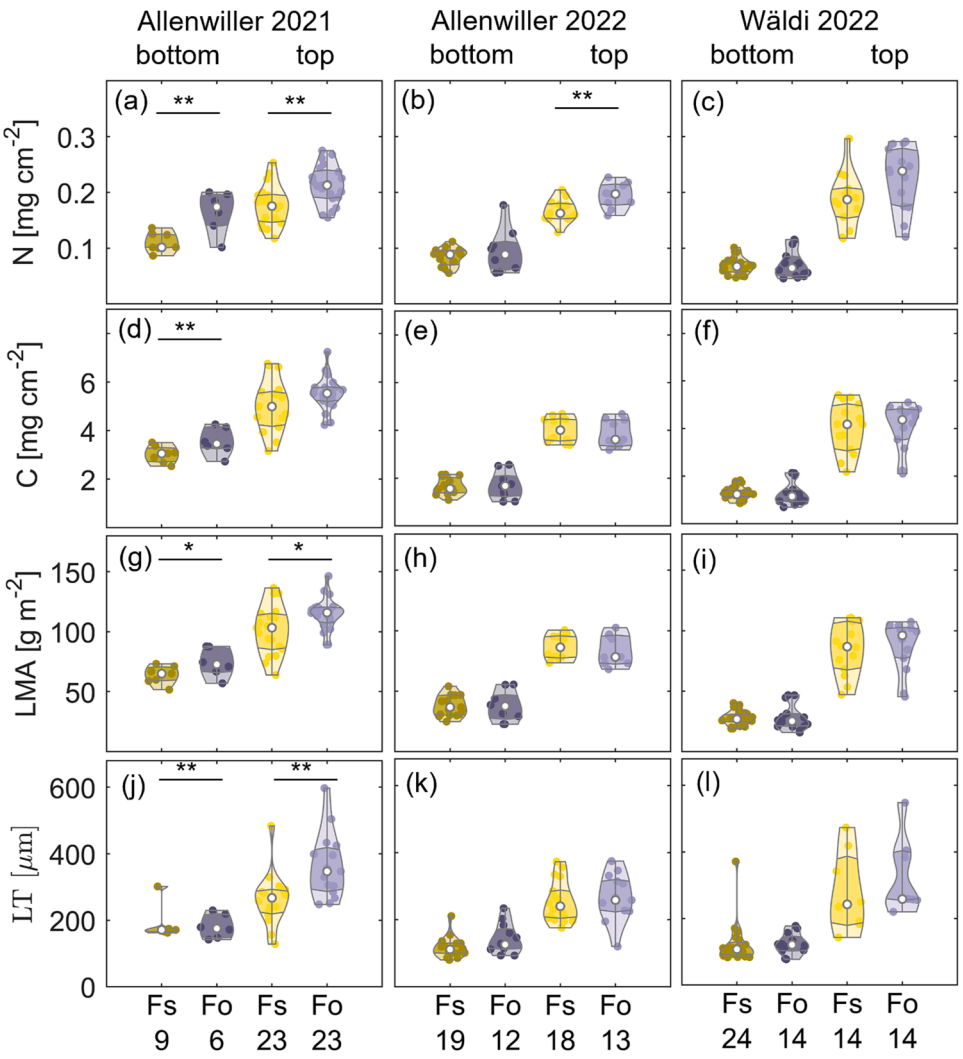

Fig. 6. Leaf traits of *F. sylvatica* (Fs) and *F. orientalis* (Fo) tree subspecies in Allenwiller, France (summer 2021 and 2022) and Wäldi, Switzerland (summer 2022). Violin plots show trait distributions, with circles representing median values and darker-colored areas representing the intervals between the 25th and 75th quartiles. The number of samples for each subspecies (Fs, Fo) is indicated under the species label. Asterisks above the violin plots indicate significant differences between subspecies at either bottom or top of canopy (* $p \leq 0.05$, ** $p \leq 0.01$, *** $p \leq 0.001$) according to linear mixed effect models, with subspecies as fixed effect and diameter at breast height class as random effect (for Allenwiller 2021 tree ID was additionally considered as random effect in the model). Leaf traits: nitrogen per unit leaf area (N; a-c), carbon per unit leaf area (C; d-f), leaf mass per area (LMA; g-i), leaf thickness (LT; j-l).

plasticity of morphological traits in Oriental beech (Table S4). Irradiance and air temperature are known to affect the programming of the leaf within the bud as well as cell expansion and number of cell layers in newly emerging leaves (Poorter et al., 2009; Uemura et al., 2000). High plasticity in these morphological traits may support more rapid adaptation to future warmer and drier conditions, for instance by allowing for leaves with reduced leaf transpiration surfaces. Last but not least, Oriental beech individuals at the two examined forest stands were characterized by top-of-canopy leaves with higher N and in 2022 also higher Chl per unit leaf area, suggesting greater ability to maximize leaf photosynthetic activity than European beech for comparable leaf area (Wright et al., 2004). Notably, subspecies trait divergence at our two sites was particularly evident for leaves at the top of the canopy, where conditions can become less favorable when high irradiance occurs in combination with decreasing water availability.

4.2. *Operational implications for subspecies classification using remote sensing*

The design of future species monitoring approaches relying on spectral datasets starts from the choice of sensor and related wavelengths required for discrimination. We found reflectance in the SWIR to discriminate the two beech subspecies most effectively (BA = 0.86 ± 0.08, k = 0.72 ± 0.15; Table 3, Fig. 7), likely due to the strong influence of defined spectral features in this region, with NIR predictors outperforming only predictors in the VIS region. This suggests that future spectral screening approaches would not be required to employ expensive spectrometers acquiring over a wide range of wavelengths, but could instead be limited to instruments measuring in a few SWIR bands. Narrowing down to the most conservative set of predictors can further facilitate the transition to airborne and satellite-based sensors that usually acquire in fewer bands.

The majority of studies using spectral data for species discrimination focused on differences in productivity among functional groups and thus built on information in the visible near-infrared (VNIR) region, governed by strong pigment absorption at the leaf level and structure at the canopy scale (as reviewed by Ustin and Gamon, 2010; Fassnacht et al., 2016). Fewer investigations concentrated on light-plant interactions in the SWIR. For example, Buitrago and colleagues (2018) found the SWIR region to accurately (k = 0.93) differentiate 19 herbaceous and woody species of different taxonomic families, spanning from the tropics to temperate regions. The authors found similar performance when using the mid-wave (2.5–6 μm) and long-wave (6–20 μm) infrared, which, however, have the drawback of rarely being available in current field, airborne and spaceborne sensors. Further studies in (sub-)tropical forests corroborate the improvement in species spectral separability obtained using the SWIR region in comparison to information in the VNIR (Bao et al., 2021); improvement that was also observed by Ferreira and colleagues (2019) at the canopy scale, leveraging new SWIR sensing capabilities offered by the WorldView-3 satellite sensor. Worth mentioning are also full spectrum transformation approaches such as wavelet transforms (Jach 2016), which was used as a discriminant

Table 2
Summary of the analysis of variance using linear mixed effect models having spectra-derived or lab traits for top or bottom of canopy leaves as the response variable, subspecies as the fixed factor and tree diameter at breast height class as random factor influencing the model intercept. The model for the Allenwiller 2021 dataset further includes tree ID as random factor to account for pseudoreplication on tree level.

Response variable	**Allenwiller 2021**			**Allenwiller 2022**			**Wäldi 2022**		
Top of canopy	N = 46			N = 31			N = 28		
Spectral traits	*F*	*p*	*d*	*F*	*p*	*d*	*F*	*p*	*d*
sN	50.4	**<0.001**	2.25	5.6	**0.024**	0.77	14.2	**<0.001**	1.35
sLig	65.8	**<0.001**	2.62	9.1	**0.005**	1.06	8.3	**0.008**	1.11
sCell	3.4	0.073	0.63	5.7	**0.024**	−0.99	1.0	0.331	−0.36
sLMA	13.2	**<0.001**	1.21	0.4	0.526	−0.33	0.1	0.788	0.14
sWater	8.2	**0.006**	0.91	1.9	0.172	−0.50	0.2	0.685	−0.11
sWax	1.9	0.171	0.37	0.4	0.515	0.09	7.5	**0.012**	1.01
sChl	2.6	0.114	0.42	7.6	**0.010**	0.86	26.2	**<0.001**	1.88
sChlCar	4.3	**0.044**	−0.60	<0.1	0.992	0.06	10.3	**0.003**	−1.18
sAnth	0.4	0.550	−0.13	5.9	**0.022**	−0.86	1.2	0.275	0.41
Lab traits									
N [mg cm^{-2}]	10.35	**0.003**	1.03	16.26	**0.001**	1.19	3.4	0.077	0.72
C [mg cm^{-2}]	2.39	0.13	0.60	0.22	0.641	−0.26	0.07	0.791	0.02
LMA [g m^{-2}]	4.1	**0.05**	0.75	0.09	0.773	−0.19	0	0.985	0.11
LT [μm]	9.89	**0.004**	1.10	0.23	0.637	0.17	1.96	0.185	0.42
Bottom of canopy	N = 15			N = 31			N = 38		
Spectral traits	*F*	*p*	*d*	*F*	*p*	*d*	*F*	*p*	*d*
sN	1.9	0.194	0.70	1.1	0.312	0.35	0.8	0.388	0.42
sLig	11.1	**0.005**	1.23	1.5	0.237	0.41	<0.1	0.864	0.23
sCell	0.4	0.544	−0.41	1.4	0.239	−0.41	18.4	**<0.001**	−1.41
sLMA	4.6	**0.050**	1.04	0.1	0.741	−0.14	<0.1	0.932	0.05
sWater	4.4	0.055	1.09	0.2	0.651	−0.17	3.7	0.063	−0.64
sWax	4.2	0.060	0.46	2.0	0.170	0.51	0.2	0.686	−0.08
sChl	1.0	0.346	0.59	5.3	**0.029**	0.82	0.1	0.785	0.23
sChlCar	1.5	0.243	−0.51	2.3	0.142	−0.54	0.1	0.806	0.01
sAnth	1.2	0.290	−0.65	0.3	0.614	0.18	1.2	0.280	0.36
Lab traits									
N [mg cm^{-2}]	31.37	**0.002**	1.73	1.16	0.292	0.36	0.14	0.711	0.18
C [mg cm^{-2}]	10.78	**0.007**	1.07	0.09	0.77	0.08	0.01	0.938	0.02
LMA [g m^{-2}]	7.49	**0.019**	0.97	0.01	0.937	−0.04	0	0.968	0.06
LT [μm]	13.79	**0.005**	−0.26	3.91	0.058	0.70	0.04	0.851	0.03

N: number of sampled trees; LMA: leaf mass per area; LT: leaf thickness; *F*: F-values from Fisher's test; *p*: p-values showed in bold when $p < 0.05$; d: Cohen's d effect size (d = 0.20 small effect, d = 0.50 medium effect, d = 0.80 large effect).

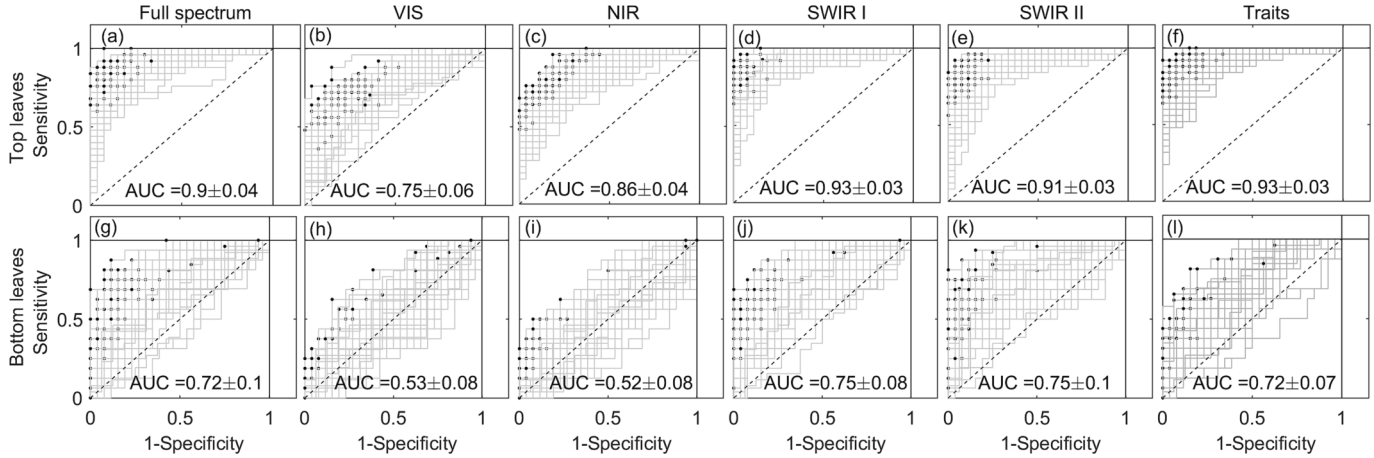

Fig. 7. Receiver operating characteristic (ROC) prediction curves calculated from the partial least square discriminant analysis (PLS-DA) of two beech subspecies (*F. orientalis; F. sylvatica*) based on spectra of leaves at the top (a-f) and bottom (g-l) of the canopy acquired in Allenwiller, France (summer 2021 and 2022) and Wäldi, Switzerland (summer 2022). Six models, differing in predictor variables: full spectra (400–2400 nm; a, g), VIS spectra (400–750 nm; b, h), NIR spectra (750–1300 nm; c, i), SWIR I spectra (1450–1750 nm; d, j) and SWIR II spectra (1950 – 2400 nm; e, k) and a set of 9 spectra-derived traits (f, l; see Table 1 for list of traits), are compared. Curves are displayed for 100 model iterations, each based on a new validation set corresponding to 50% of total samples. Black dots represent optimal threshold values, minimizing omission (sensitivity) and commission (1-specificity) errors. The mean ROC Area Under the Curve (AUC; ± 1 std) are given over the 100 model iterations.

Table 3
Partial least square discriminant analysis (PLS-DA) prediction statistics of two beech subspecies (*F. orientalis*; *F. sylvatica*) based on spectra of leaves at the top (N = 105) and bottom (N = 84) of the canopy sampled in Allenwiller, France (summer 2021 and 2022) and Wäldi, Switzerland (summer 2022). Six models, using either the full spectrum (400–2400 nm) or a range of wavelengths or a set of 9 spectra-derived traits (see Table 1 for list of traits), are compared. Performance metrics are averaged over 100 model iterations, each based on a new validation set corresponding to 50% of total samples.

Predictors	Top-of-canopy			Bottom-of-canopy		
	BA (mean ± 1std)	k (mean ± 1std)	na [%]	BA (mean ± 1std)	k (mean ± 1std)	na [%]
Full spectrum: 400 – 2400 nm	0.82 ± 0.05	0.63 ± 0.09	2O 3 S	0.64 ± 0.13	0.28 ± 0.25	5O 2 S
VIS: 400 – 750 nm	0.71 ± 0.07	0.40 ± 0.13	4O 3S	0.50 ± 0.07	< 0.1	8O 3S
NIR: 750 – 1300 nm	0.76 ± 0.07	0.51 ± 0.13	2O 1S	0.51 ± 0.07	< 0.1	6O 3S
SWIR I: 1450 –1750 nm	0.86 ± 0.08	0.72 ± 0.15	4O 1S	0.68 ± 0.12	0.34 ± 0.23	7O 3S
SWIR II: 1950 –2400 nm	0.85 ± 0.05	0.69 ± 0.10	3O 3S	0.67 ± 0.14	0.34 ± 0.26	8O 3S
Spectra-derived traits	0.84 ± 0.05	0.67 ± 0.10	0O 0 S	0.56 ± 0.09	0.12 ± 0.17	0O 0 S

VIS: visible; NIR: near-infrared; SWIR: shortwave infrared; O: *F. orientalis*; S: *F. sylvatica*. BA: balanced accuracy (ranges from 0 worst to 1 best); k: kappa statistics (<0 poor, 0.00–0.20 slight, 0.21–0.40 fair, 0.41–0.60 moderate, 0.61–0.80 substantial, 0.81–1.00 high (Landis and Koch, 1977)); na: not assigned samples in %.

analysis precursor in classification studies employing airborne hyperspectral data, from pine species (Banskota et al., 2011) to tropical tree species (Zhang et al., 2006).

4.3. Future lines of research

In this study, we examined spectral and functional differences between European and Oriental beech at two central European forest stands both having the same Greater Caucasian provenance of Oriental beech, and thus not covering the entire trait distribution of the subspecies across their natural ranges. European beech is characterized by high phenotypic plasticity, and studies based on provenance trials have found adaptive response capability encompassing several traits associated with phenology, growth, and resistance to drought (Bresson et al., 2011; Frank et al., 2017; Müller et al., 2020; Stojnić et al., 2015). Among these are also morphological leaf traits, such as LMA and LT which, in a study by Stojnic and colleagues (2015), were found to vary among European beech provenances grown under marginal conditions. Interestingly, the same authors indicated that adaptation to unfavorable growth conditions was not necessarily associated with beech provenances from southern and dry sites, but instead observed for certain Central and Eastern European provenances originating from mesic sites. This reinforces the fact that identification and use of appropriate beech seed sources for assisted migration requires a *priori* evaluation that is best achieved through high-throughput phenotyping approaches, like the one presented in this study based on spectral data, in combination with multi-provenance plantation networks spanning a wide range of environmental conditions. Notably, these networks should include marginal sites, where environmental filtering effects and phenotypic plasticity shape the tails of trait distributions (Gárate-Escamilla et al., 2019). The network of Oriental beech planting sites identified by Kurz and colleagues (2023) could be exploited for further physiological phenotyping, especially because Oriental beech provenances other than the Greater Caucasian are also present in this network.

Although this study focused on leaf spectroscopy for subspecies discrimination, it has clear implications for crown-level tree classifications from airborne or satellite-based imagery. Findings of this study provide a starting point for the interpretation of variability in tree crown reflectance. The superior discrimination capacity of leaves at the top of the canopy as compared to bottom-of-canopy leaves holds promise for the upscaling of the method using remote sensing. Unlike leaf spectra, tree crown spectra are influenced by background signals and acquisition geometry that might challenge classification, and by canopy structure (e.g., leaf area index, crown shape) which, for species that have unique and predictable combination of these parameters, could support classification at the crown level. In this respect, combining foliar biochemistry retrieved from optical data with structural information obtained from LiDAR (Light Detection And Ranging) sensors onboard UAVs or other aerial platforms could further extend classification possibilities (Li et al., 2013).

We foresee using spectral data to investigate the genetic and phenotypic clines between European and Oriental beech. Given the relatively young age of our two study sites, no mature hybrid individuals were identified following the genetic analysis. Yet, a testbed for this evaluation can be found in the natural hybrid zone in Bulgaria, where natural distribution ranges of the two subspecies overlap, resulting in all the complexity of an ongoing hybridization (Denk et al., 2002; Vettori et al., 2004). A spectral phenotyping approach allowing to monitor the rate of hybridization between native and introduced species, in addition to their resilience, would represent an important support tool for assisted migration programs.

5. Conclusions

The introduction of close relatives of native species, or of populations from different parts of the species range, to our forests as a climate change mitigation strategy presents challenges for monitoring due to similarities in appearance of introduced and native trees. Traditional ground-based phenotyping methods and expensive, laborious genetic screening alone are not sufficient for monitoring across large geographic areas. Our work shows that leaf spectroscopy, particularly leaf reflectance spectra in the short-wave-infrared (SWIR), was able to accurately discriminate individuals of European and Oriental beech subspecies, growing under the same environmental conditions at two 100-year-old central European forest stands. Discrimination capacity was mainly linked with higher spectra-derived lignin and protein-N found in Oriental beech leaves as compared to European beech, influencing leaf optical properties directly through constituents' absorption features in the SWIR and indirectly via their relationship with structural leaf traits. The superior discrimination capacity of leaves at the top of the canopy, as compared to bottom-of-canopy leaves, indicates the importance of environmental interactions in revealing these differences and holds promise for the upscaling of the method using airborne or spaceborne remote sensing. The presented proof-of-principle for discriminating subspecies could, in future, allow monitoring of other newly introduced species, as well as hybridization rates and spread of adaptive genetic variants upon assisted gene flow, and further improve our understanding of their functional adaptation strategies based on spectral data.

CRediT authorship contribution statement

Petra D'Odorico: Conceptualization, Funding acquisition, Resources, Investigation, Methodology, Data curation, Formal analysis, Visualization, Writing – original draft, Writing – review & editing. **Meredith C. Schuman:** Conceptualization, Funding acquisition, Resources, Project administration, Supervision, Investigation, Methodology, Data curation, Writing – review & editing. **Mirjam Kurz:** Data curation, Formal analysis. **Katalin Csilléry:** Conceptualization, Funding acquisition, Resources, Project administration, Supervision, Investigation, Methodology, Data curation, Formal analysis, Writing – review & editing.

Declaration of Competing Interest

The authors declare that they have no known competing financial interests or personal relationships that could have appeared to influence the work reported in this paper.

Data availability

All the data supporting the findings of this study is available in the WSL's Environmental Data Portal (EnviDat) [https://doi.org/10.16904/envidat.390].

Acknowledgements

This work was supported by a SwissForestLab grant (SFL-20 P6). KC holds an ERC Consolidator Grant "MyGardenOfTrees" (101003296), which supported her during this project. MCS acknowledges support by the URPP Global Change and Biodiversity program.

We are thankful to Alexander Steppke for supporting sampling and developing the leaf thickness meter, and to Didier Le-Thiec for coordination and support at Allenwiller. We further like to thank Beatriz Pablo Carmona, Nemish Murawat, Adrian Kölz, Valeska Holenstein, Nadiia Matus, David Combemale and Cyril Bure for contributing to lab or field work. We thank two anonymous reviewers for their valuable comments on the manuscript.

Appendix A. Supplementary material

Supplementary data to this article can be found online at https://doi.org/10.1016/j.foreco.2023.121056.

References

Abràmoff, D.M.D., Magalhães, D.P.J., Ram, D.S.J., 2004. Image Processing with ImageJ <p>. Biophotonics Int. 11 (7), 36–42.

Aitken, S.N., Bemmels, J.B., 2016. Time to get moving: assisted gene flow of forest trees. Evol. Appl. 9 (1), 271–290. https://doi.org/10.1111/eva.12293.

Aitken, S.N., Whitlock, M.C., 2013. Assisted gene flow to facilitate local adaptation to climate change. Annu. Rev. Ecol. Evol. Syst. 44 (1), 367–388. https://doi.org/10.1146/annurev-ecolsys-110512-135747.

Aitken, S.N., Yeaman, S., Holliday, J.A., Wang, T., Curtis-McLane, S., 2008. Adaptation, migration or extirpation: climate change outcomes for tree populations. Evol. Appl. 1 (1), 95–111. https://doi.org/10.1111/j.1752-4571.2007.00013.x.

Anderegg, W.R.L., Anderegg, L.D.L., Kerr, K.L., Trugman, A.T., 2019. Widespread drought-induced tree mortality at dry range edges indicates that climate stress exceeds species' compensating mechanisms. Glob. Chang. Biol. 25 (11), 3793–3802. https://doi.org/10.1111/gcb.14771.

Anderson, J.T., Wadgymar, S.M., 2020. Climate change disrupts local adaptation and favours upslope migration. Ecol Lett 23, 181–192. https://doi.org/10.1111/ele.13427.

Asner, G.P., Knapp, D.E., Kennedy-Bowdoin, T., Jones, M.O., Martin, R.E., Boardman, J., Hughes, R.F., 2008. Invasive species detection in Hawaiian rainforests using airborne imaging spectroscopy and LiDAR. Remote Sens. Environ. 112 (5), 1942–1955. https://doi.org/10.1016/j.rse.2007.11.016.

Asner, G.P., Martin, R.E., 2011. Canopy phylogenetic, chemical and spectral assembly in a lowland Amazonian forest. New Phytol. 189 (4), 999–1012. https://doi.org/10.1111/j.1469-8137.2010.03549.x.

Asner, G.P., Martin, R.E., Keith, L.M., Heller, W.P., Hughes, M.A., Vaughn, N.R., Balzotti, C., 2018. Spectral Mapping Signature for the Rapid Ohia Death Pathogen in Hawaiian Forests. Remote Sens. (Basel) 10 (3).

Bachofen, C., D'Odorico, P., Buchmann, N., 2020. Light and VPD gradients drive foliar nitrogen partitioning and photosynthesis in the canopy of European beech and silver fir. Oecologia 192 (2), 323–339. https://doi.org/10.1007/s00442-019-04583-x.

Ballabio, D., Consonni, V., 2013. Classification tools in chemistry. Part 1: linear models. PLS-DA [10.1039/C3AY40582F]. Anal. Methods 5 (16), 3790–3798. https://doi.org/10.1039/C3AY40582F.

Banskota, A., Wynne, R.H., Kayastha, N., 2011. Improving within-genus tree species discrimination using the discrete wavelet transform applied to airborne hyperspectral data. Int. J. Remote Sens. 32 (13), 3551–3563. https://doi.org/10.1080/01431161003698302.

Bao, S., Cao, C., Chen, W., Yang, T., Wu, C., 2021. Towards a subtropical forest spectral library: spectra consistency and spectral separability. Geocarto Int. 36 (2), 226–240. https://doi.org/10.1080/10106049.2019.1608589.

Bogunović, S., Bogdan, S., Lanšćak, M., Ćelepirović, N., Ivanković, M., 2020. Use of a common garden experiment in selecting adapted beech provenances for artificial stand restoration. South-east European forestry: SEEFOR 11 (1), 1–10.

Bresson, C.C., Vitasse, Y., Kremer, A., Delzon, S., 2011. To what extent is altitudinal variation of functional traits driven by genetic adaptation in European oak and beech? Tree Physiol. 31 (11), 1164–1174. https://doi.org/10.1093/treephys/tpr084.

Buitrago, M.F., Skidmore, A.K., Groen, T.A., Hecker, C.A., 2018. Connecting infrared spectra with plant traits to identify species. ISPRS J. Photogramm. Remote Sens. 139, 183–200. https://doi.org/10.1016/j.isprsjprs.2018.03.013.

Camarillo-Castillo, F., Huggins, T.D., Mondal, S., Reynolds, M.P., Tilley, M., Hays, D.B., 2021. High-resolution spectral information enables phenotyping of leaf epicuticular wax in wheat. Plant Methods 17 (1), 58. https://doi.org/10.1186/s13007-021-00759-w.

Cardoni, S., Piredda, R., Denk, T., Grimm, G.W., Papageorgiou, A.C., Schulze, E.-D., Cosimo Simeone, M., 2022. 5S-IGS rDNA in wind-pollinated trees (Fagus L.) encapsulates 55 million years of reticulate evolution and hybrid origins of modern species. Plant J. 109 (4), 909–926. https://doi.org/10.1111/tpj.15601.

Castro-Esau, K.L., Sánchez-Azofeifa, G.A., Rivard, B., Wright, S.J., Quesada, M., 2006. Variability in leaf optical properties of Mesoamerican trees and the potential for species classification. Am. J. Bot. 93 (4), 517–530. https://doi.org/10.3732/ajb.93.4.517.

Cavender-Bares, J., Meireles, J.E., Couture, J.J., Kaproth, M.A., Kingdon, C.C., Singh, A., Townsend, P.A., 2016. Associations of leaf spectra with genetic and phylogenetic variation in oaks: prospects for remote detection of biodiversity. Remote Sens. (Basel) 8 (3). https://doi.org/10.3390/rs8030221.

Cavender-Bares, J., Schneider, F.D., Santos, M.J., Armstrong, A., Carnaval, A., Dahlin, K. M., Wilson, A.M., 2022. Integrating remote sensing with ecology and evolution to advance biodiversity conservation. Nat. Ecol. Evol. 6 (5), 506–519. https://doi.org/10.1038/s41559-022-01702-5.

Charron, G., Robichaud-Courteau, T., La Vigne, H., Weintraub, S., Hill, A., Justice, D., Lussier Desbiens, A., 2020. The DeLeaves: a UAV device for efficient tree canopy sampling. J. Unmanned Vehicle Systems 8 (3), 245–264. https://doi.org/10.1139/juvs-2020-0005.

Chevallier, S., Bertrand, D., Kohler, A., Courcoux, P., 2006. Application of PLS-DA in multivariate image analysis. J. Chemom. 20 (5), 221–229. https://doi.org/10.1002/cem.994.

Clark, M.L., Roberts, D.A., Clark, D.B., 2005. Hyperspectral discrimination of tropical rain forest tree species at leaf to crown scales. Remote Sens. Environ. 96 (3), 375–398. https://doi.org/10.1016/j.rse.2005.03.009.

Cohen, J., 1960. A coefficient of agreement for nominal scales. Educ. Psychol. Meas. 20 (1), 37–46. https://doi.org/10.1177/001316446002000104.

Corlett, R.T., Westcott, D.A., 2013. Will plant movements keep up with climate change? Trends Ecol. Evol. 28 (8), 482–488. https://doi.org/10.1016/j.tree.2013.04.003.

Curran, P.J., 1989. Remote sensing of foliar chemistry. Remote Sens. Environ. 30 (3), 271–278. https://doi.org/10.1016/0034-4257(89)90069-2.

Czyż, E.A., Guillén Escribà, C., Wulf, H., Tedder, A., Schuman, M.C., Schneider, F.D., Schaepman, M.E., 2020. Intraspecific genetic variation of a Fagus sylvatica population in a temperate forest derived from airborne imaging spectroscopy time series. Ecol. Evol. 10 (14), 7419–7430. https://doi.org/10.1002/ece3.6469.

Datt, B., 1999. Visible/near infrared reflectance and chlorophyll content in Eucalyptus leaves. Int. J. Remote Sens. 20 (14), 2741–2759. https://doi.org/10.1080/014311699211778.

Daughtry, C.S.T., Hunt, E.R., McMurtrey, J.E., 2004. Assessing crop residue cover using shortwave infrared reflectance. Remote Sens. Environ. 90 (1), 126–134. https://doi.org/10.1016/j.rse.2003.10.023.

Denk, T., Grimm, G., Stögerer, K., Langer, M., Hemleben, V., 2002. The evolutionary history of Fagus in western Eurasia: evidence from genes, morphology and the fossil record. Plant Syst. Evol. 232 (3), 213–236. https://doi.org/10.1007/s006060200044.

D'Odorico, P., Schönbeck, L., Vitali, V., Meusburger, K., Schaub, M., Ginzler, C., Zweifel, R., Velasco, V.M.E., Gisler, J., Gessler, A., Ensminger, I., 2021. Drone-based physiological index reveals long-term acclimation and drought stress responses in trees. Plant Cell Environ. 44 (11), 3552–3570. https://doi.org/10.1111/pce.14177.

Durán, S.M., Martin, R.E., Díaz, S., Maitner, B.S., Malhi, Y., Salinas, N., Enquist, B.J., 2019. Informing trait-based ecology by assessing remotely sensed functional diversity across a broad tropical temperature gradient. *Science*. Advances 5 (12), eaaw8114. https://doi.org/10.1126/sciadv.aaw8114.

Earl, D.A., vonHoldt, B.M., 2012. STRUCTURE HARVESTER: a website and program for visualizing STRUCTURE output and implementing the Evanno method. Conserv. Genet. Resour. 4 (2), 359–361. https://doi.org/10.1007/s12686-011-9548-7.

Ely, K.S., Burnett, A.C., Lieberman-Cribbin, W., Serbin, S.P., Rogers, A., 2019. Spectroscopy can predict key leaf traits associated with source–sink balance and carbon–nitrogen status. J. Exp. Bot. 70 (6), 1789–1799. https://doi.org/10.1093/jxb/erz061.

Evanno, G., Regnaut, S., Goudet, J., 2005. Detecting the number of clusters of individuals using the software structure: a simulation study. Mol. Ecol. 14 (8), 2611–2620. https://doi.org/10.1111/j.1365-294X.2005.02553.x.

Fang, J., Lechowicz, M.J., 2006. Climatic limits for the present distribution of beech (Fagus L.) species in the world. J. Biogeogr. 33 (10), 1804–1819. https://doi.org/10.1111/j.1365-2699.2006.01533.x.

Fassnacht, F.E., Latifi, H., Stereńczak, K., Modzelewska, A., Lefsky, M., Waser, L.T., Ghosh, A., 2016. Review of studies on tree species classification from remotely sensed data. Remote Sens. Environ. 186, 64–87. https://doi.org/10.1016/j.rse.2016.08.013.

Féret, J.-B., François, C., Gitelson, A., Asner, G.P., Barry, K.M., Panigada, C., Jacquemoud, S., 2011. Optimizing spectral indices and chemometric analysis of leaf chemical properties using radiative transfer modeling. Remote Sens. Environ. 115 (10), 2742–2750. https://doi.org/10.1016/j.rse.2011.06.016.

Féret, J.-B., Berger, K., de Boissieu, F., Malenovský, Z., 2021. PROSPECT-PRO for estimating content of nitrogen-containing leaf proteins and other carbon-based constituents. Remote Sens. Environ. 252, 112173 https://doi.org/10.1016/j.rse.2020.112173.

Ferreira, M.P., Wagner, F.H., Aragão, L.E.O.C., Shimabukuro, Y.E., de Souza Filho, C.R., 2019. Tree species classification in tropical forests using visible to shortwave infrared WorldView-3 images and texture analysis. ISPRS J. Photogramm. Remote Sens. 149, 119–131. https://doi.org/10.1016/j.isprsjprs.2019.01.019.

Forzieri, G., Girardello, M., Ceccherini, G., et al., 2021. Emergent vulnerability to climate-driven disturbances in European forests. Nat. Commun. 12, 1081. https://doi.org/10.1038/s41467-021-21399-7.

Fourty, T., Baret, F., Jacquemoud, S., Schmuck, G., Verdebout, J., 1996. Leaf optical properties with explicit description of its biochemical composition: direct and inverse problems. Remote Sens. Environ. 56 (2), 104–117. https://doi.org/10.1016/0034-4257(95)00234-0.

Frank, A., Pluess, A.R., Howe, G.T., Sperisen, C., Heiri, C., 2017. Quantitative genetic differentiation and phenotypic plasticity of European beech in a heterogeneous landscape: Indications for past climate adaptation. Perspectives in Plant Ecol. Evolution and Systematics 26, 1–13. https://doi.org/10.1016/j.ppees.2017.02.001.

Frei, E. R., Gossner, M. M., Vitasse, Y., Queloz, V., Dubach, V., Gessler, A., . . . Wohlgemuth, T. 2022. European beech dieback after premature leaf senescence during the 2018 drought in northern Switzerland. *Plant Biology*, *n/a*(n/a). 10.1111/plb.13467.

Gamon, J.A., Huemmrich, K.F., Wong, C.Y.S., Ensminger, I., Garrity, S., Hollinger, D.Y., Peñuelas, J., 2016. A remotely sensed pigment index reveals photosynthetic phenology in evergreen conifers. Proc. Natl. Acad. Sci. 113 (46), 13087. https://doi.org/10.1073/pnas.1606162113.

Gao, B.-C., 1996. NDWI—A normalized difference water index for remote sensing of vegetation liquid water from space. Remote Sens. Environ. 58 (3), 257–266. https://doi.org/10.1016/S0034-4257(96)00067-3.

Gárate-Escamilla, H., Hampe, A., Vizcaíno-Palomar, N., Robson, T.M., Benito Garzón, M., 2019. Range-wide variation in local adaptation and phenotypic plasticity of fitness-related traits in Fagus sylvatica and their implications under climate change. Global Ecol Biogeogr. 28, 1336–1350. https://doi.org/10.1111/geb.12936.

Geßler, A., Keitel, C., Kreuzwieser, J., Matyssek, R., Seiler, W., Rennenberg, H., 2007. Potential risks for European beech (Fagus sylvatica L.) in a changing climate. Trees 21 (1), 1–11. https://doi.org/10.1007/s00468-006-0107-x.

Gitelson, A.A., Merzlyak, M.N., Chivkunova, O.B., 2001. Optical properties and nondestructive estimation of anthocyanin content in plant leaves. Photochem. Photobiol. 74 (1), 38–45.

Grummer, J.A., Booker, T.R., Matthey-Doret, R., Nietlisbach, P., Thomaz, A.T., Whitlock, M.C., 2022. The immediate costs and long-term benefits of assisted gene flow in large populations. Conserv. Biol. 36, e13911.

Hällfors, M.H., Vaara, E.M., Hyvärinen, M., Oksanen, M., Schulman, L.E., Siipi, H., et al., 2014. Coming to terms with the concept of moving species threatened by climate change – A systematic review of the terminology and definitions. PLoS One 9 (7), e102979.

Hikosaka, K., 2004. Interspecific difference in the photosynthesis–nitrogen relationship: patterns, physiological causes, and ecological importance. J. Plant Res. 117 (6), 481–494. https://doi.org/10.1007/s10265-004-0174-2.

Hikosaka, K., Terashima, I., 1996. Nitrogen partitioning among photosynthetic components and its consequence in sun and shade plants. Funct. Ecol. 10 (3), 335–343. https://doi.org/10.2307/2390281.

Hueni, A., Bialek, A., 2017. Cause, effect, and correction of field spectroradiometer interchannel radiometric steps. IEEE J. Sel. Top. Appl. Earth Obs. Remote Sens. 10 (4), 1542–1551. https://doi.org/10.1109/JSTARS.2016.2625043.

Jach, A., 2016. (2015) Solar spectrum through the wavelet lens, UV4Plants Bulletin. Helsinki, Finland 2, 33–36. https://doi.org/10.19232/uv4pb.2016.2.14.

Jump, A.S., Hunt, J.M., PeÑUelas, J., 2006. Rapid climate change-related growth decline at the southern range edge of Fagus sylvatica. Glob. Chang. Biol. 12 (11), 2163–2174. https://doi.org/10.1111/j.1365-2486.2006.01250.x.

Kandemir, G., & Kaya, Z. 2009. EUFORGEN: Technical guidelines for genetic conservation and use for oriental beech (Fagus orientalis). *6*.

Klein, H. 1981. Le hêtre d'Orient d'Allenwiller. In: Bulletin Du Jardin Botanique de Saverne.

Klesse, S., Wohlgemuth, T., Meusburger, K., Vitasse, Y., von Arx, G., Lévesque, M., Frei, E.R., 2022. Long-term soil water limitation and previous tree vigor drive local variability of drought-induced crown dieback in Fagus sylvatica. Sci. Total Environ. 851, 157926 https://doi.org/10.1016/j.scitotenv.2022.157926.

Kokaly, R.F., 2001. Investigating a physical basis for spectroscopic estimates of leaf nitrogen concentration. Remote Sens. Environ. 75 (2), 153–161. https://doi.org/10.1016/S0034-4257(00)00163-2.

Kokaly, R.F., Asner, G.P., Ollinger, S.V., Martin, M.E., Wessman, C.A., 2009. Characterizing canopy biochemistry from imaging spectroscopy and its application to ecosystem studies. Remote Sens. Environ. 113, S78–S91. https://doi.org/10.1016/j.rse.2008.10.018.

Kopelman, N.M., Mayzel, J., Jakobsson, M., Rosenberg, N.A., Mayrose, I., 2015. Clumpak: a program for identifying clustering modes and packaging population structure inferences across K. Mol. Ecol. Resour. 15 (5), 1179–1191. https://doi.org/10.1111/1755-0998.12387.

Kothari, S., Beauchamp-Rioux, R., Laliberté, E., Cavender-Bares, J., 2023b. Reflectance spectroscopy allows rapid, accurate and non-destructive estimates of functional traits from pressed leaves. Methods Ecol. Evol. 14, 385–401. https://doi.org/10.1111/2041-210X.13958.

Kothari, S., Schweiger, A.K., 2022. Plant spectra as integrative measures of plant phenotypes. J. Ecol. 110, 2536–2554. https://doi.org/10.1111/1365-2745.13972.

Kothari, S., Beauchamp-Rioux, R., Blanchard, F., Crofts, A.L., Girard, A., Guilbeault-Mayers, X., Hacker, P.W., Pardo, J., Schweiger, A.K., Demers-Thibeault, S., Bruneau, A., Coops, N.C., Kalacska, M., Vellend, M., Laliberté, E., 2023a. Predicting leaf traits across functional groups using reflectance spectroscopy. New Phytol. 238, 549–566. https://doi.org/10.1111/nph.18713.

Kozhoridze, G., Orlovsky, N., Orlovsky, L., Blumberg, D.G., Golan-Goldhirsh, A., 2016. Remote sensing models of structure-related biochemicals and pigments for classification of trees. Remote Sens. Environ. 186, 184–195. https://doi.org/10.1016/j.rse.2016.08.024.

Kurz, M., Kölz, A., Gorges, J., Pablo Carmona, B., Brang, P., Vitasse, Y., Csilléry, K., 2023. Tracing the origin of Oriental beech stands across Western Europe and reporting hybridization with European beech – Implications for assisted gene flow. For. Ecol. Manage. 531, 120801 https://doi.org/10.1016/j.foreco.2023.120801.

Landis, J.R., Koch, G.G., 1977. The measurement of observer agreement for categorical data. Biometrics 33 (1), 159–174. https://doi.org/10.2307/2529310.

le Maire, G., François, C., Dufrêne, E., 2004. Towards universal broad leaf chlorophyll indices using PROSPECT simulated database and hyperspectral reflectance measurements. Remote Sens. Environ. 89 (1), 1–28. https://doi.org/10.1016/j.rse.2003.09.004.

Lefèvre, S., Wagner, S., Petit, R.J., De Lafontaine, G., 2012. Multiplexed microsatellite markers for genetic studies of beech. Mol. Ecol. Resour. 12 (3), 484–491. https://doi.org/10.1111/j.1755-0998.2011.03094.x.

Li, J., Hu, B., Noland, T.L., 2013. Classification of tree species based on structural features derived from high density LiDAR data. Agric. For. Meteorol. 171–172, 104–114. https://doi.org/10.1016/j.agrformet.2012.11.012.

Madritch, M.D., Kingdon, C.C., Singh, A., Mock, K.E., Lindroth, R.L., Townsend, P.A., 2014. Imaging spectroscopy links aspen genotype with below-ground processes at landscape scales. Philos. Trans. R. Soc., B 369 (1643), 20130194. https://doi.org/10.1098/rstb.2013.0194.

Martinez del Castillo, E., Zang, C.S., Buras, A., Hacket-Pain, A., Esper, J., Serrano-Notivoli, R., de Luis, M., 2022. Climate-change-driven growth decline of European beech forests. Commun. Biol. 5 (1), 163. https://doi.org/10.1038/s42003-022-03107-3.

McLachlan, J.S., Hellmann, J.J., Schwartz, M.W., 2007. A framework for debate of assisted migration in an era of climate change. Conserv. Biol. 21 (2), 297–302. https://doi.org/10.1111/j.1523-1739.2007.00676.x.

Meireles, J.E., Cavender-Bares, J., Townsend, P.A., Ustin, S., Gamon, J.A., Schweiger, A. K., O'Meara, B.C., 2020. Leaf reflectance spectra capture the evolutionary history of seed plants. New Phytol. 228 (2), 485–493. https://doi.org/10.1111/nph.16771.

Mellert, K.H., Seho, M., 2022. Suitability of Fagus orientalis Lipsky at marginal Fagus sylvatica L. forest sites in Southern Germany. *iForest* -. Biogeosciences and Forestry 15 (5), 417–423. https://doi.org/10.3832/ifor4077-015.

Müller, M., Kempen, T., Finkeldey, R., Gailing, O., 2020. Low population differentiation but high phenotypic plasticity of european beech in germany. Forests 11 (12).

Neumann, M., Mues, V., Moreno, A., Hasenauer, H., Seidl, R., 2017. Climate variability drives recent tree mortality in Europe. Glob. Chang. Biol. 23 (11), 4788–4797. https://doi.org/10.1111/gcb.13724.

Obladen, N., Dechering, P., Skiadaresis, G., Tegel, W., Keßler, J., Höllerl, S., Seim, A., 2021. Tree mortality of European beech and Norway spruce induced by 2018–2019 hot droughts in central Germany. Agric. For. Meteorol. 307, 108482 https://doi.org/10.1016/j.agrformet.2021.108482.

Ollinger, S.V., 2011. Sources of variability in canopy reflectance and the convergent properties of plants. New Phytol. 189 (2), 375–394. https://doi.org/10.1111/j.1469-8137.2010.03536.x.

Onoda, Y., Hikosaka, K., Hirose, T., 2004. Allocation of nitrogen to cell walls decreases photosynthetic nitrogen-use efficiency. Funct. Ecol. 18 (3), 419–425. https://doi.org/10.1111/j.0269-8463.2004.00847.x.

Peñuelas, J., Hunt, J.M., Ogaya, R., Jump, A.S., 2008. Twentieth century changes of tree-ring δ13C at the southern range-edge of Fagus Sylvatica: increasing water-use efficiency does not avoid the growth decline induced by warming at low altitudes. Glob Chang Biol 14. https://doi.org/10.1111/j.1365-2486.2008.01563.x.

Petibon, F., Czyż, E.A., Ghielmetti, G., Hueni, A., Kneubühler, M., Schaepman, M.E., Schuman, M.C., 2021. Uncertainties in measurements of leaf optical properties are small compared to the biological variation within and between individuals of European beech. Remote Sens. Environ. 264, 112601 https://doi.org/10.1016/j.rse.2021.112601.

Poorter, H., Niinemets, Ü., Poorter, L., Wright, I.J., Villar, R., 2009. Causes and consequences of variation in leaf mass per area (LMA): a meta-analysis. New Phytol. 182 (3), 565–588. https://doi.org/10.1111/j.1469-8137.2009.02830.x.

Pritchard, J.K., Stephens, M., Donnelly, P., 2000. Inference of Population Structure Using Multilocus Genotype Data. Genetics 155 (2), 945–959. https://doi.org/10.1093/genetics/155.2.945.

Schweiger, A.K., Cavender-Bares, J., Townsend, P.A., Hobbie, S.E., Madritch, M.D., Wang, R., Gamon, J.A., 2018. Plant spectral diversity integrates functional and phylogenetic components of biodiversity and predicts ecosystem function. Nat. Ecol. Evol. 2 (6), 976–982. https://doi.org/10.1038/s41559-018-0551-1.

Senf, C., Pflugmacher, D., Zhiqiang, Y., Sebald, J., Knorn, J., Neumann, M., Seidl, R., 2018. Canopy mortality has doubled in Europe's temperate forests over the last three decades. Nat. Commun. 9 (1), 4978. https://doi.org/10.1038/s41467-018-07539-6.

Serbin, S.P., Singh, A., McNeil, B.E., Kingdon, C.C., Townsend, P.A., 2014. Spectroscopic determination of leaf morphological and biochemical traits for northern temperate and boreal tree species. Ecol. Appl. 24 (7), 1651–1669. https://doi.org/10.1890/13-2110.1.

Serrano, L., Peñuelas, J., Ustin, S.L., 2002. Remote sensing of nitrogen and lignin in Mediterranean vegetation from AVIRIS data: decomposing biochemical from

structural signals. Remote Sens. Environ. 81 (2), 355–364. https://doi.org/10.1016/S0034-4257(02)00011-1.
Siefert, A., Violle, C., Chalmandrier, L., Albert, C.H., Taudiere, A., Fajardo, A., Wardle, D. A., 2015. A global meta-analysis of the relative extent of intraspecific trait variation in plant communities. Ecol. Lett. 18 (12), 1406–1419. https://doi.org/10.1111/ele.12508.
Spilke, J., Piepho, H.P., Hu, X., 2005. Analysis of unbalanced data by mixed linear models using the mixed procedure of the SAS System. J. Agron. Crop Sci. 191 (1), 47–54. https://doi.org/10.1111/j.1439-037X.2004.00120.x.
Stanke, H., Finley, A.O., Domke, G.M., Weed, A.S., MacFarlane, D.W., 2021. Over half of western United States' most abundant tree species in decline. Nat. Commun. 12 (1), 451. https://doi.org/10.1038/s41467-020-20678-z.
Stojnić, S., Orlović, S., Miljković, D., Galić, Z., Kebert, M., von Wuehlisch, G., 2015. Provenance plasticity of European beech leaf traits under differing environmental conditions at two Serbian common garden sites. Eur. J. For. Res. 134 (6), 1109–1125. https://doi.org/10.1007/s10342-015-0914-y.
Sullivan, G.M., Feinn, R., 2012. Using Effect Size—or Why the P Value Is Not Enough. J. Grad. Med. Educ. 4 (3), 279–282. https://doi.org/10.4300/JGME-D-12-00156.1.
Takashima, T., Hikosaka, K., Hirose, T., 2004. Photosynthesis or persistence: nitrogen allocation in leaves of evergreen and deciduous Quercus species. Plant Cell Environ. 27 (8), 1047–1054. https://doi.org/10.1111/j.1365-3040.2004.01209.x.
Uemura, A., Ishida, A., Nakano, T., Terashima, I., Tanabe, H., Matsumoto, Y., 2000. Acclimation of leaf characteristics of Fagus species to previous-year and current-year solar irradiances. Tree Physiol. 20 (14), 945–951. https://doi.org/10.1093/treephys/20.14.945.
Ustin, S.L., Gamon, J.A., 2010. Remote sensing of plant functional types. New Phytol. 186 (4), 795–816. https://doi.org/10.1111/j.1469-8137.2010.03284.x.
Vettori, C., Paffetti, D., Paule, L., Giannini, R., 2004. Identification of the Fagus sylvatica L. and Fagus orientalis Lipsky species and intraspecific variability. For. Genet. 10, 223–230.
Winder, R., Nelson, E., Beardmore, T., 2011. Ecological implications for assisted migration in Canadian forests. For. Chron. 87 (06), 731–744. https://doi.org/10.5558/tfc2011-090.
Wold, S., Sjöström, M., Eriksson, L., 2001. PLS-regression: a basic tool of chemometrics. Chemom. Intel. Lab. Syst. 58 (2), 109–130. https://doi.org/10.1016/S0169-7439(01)00155-1.
Wong, C.Y.S., D'Odorico, P., Bhathena, Y., Arain, M.A., Ensminger, I., 2019. Carotenoid based vegetation indices for accurate monitoring of the phenology of photosynthesis at the leaf-scale in deciduous and evergreen trees. Remote Sens. Environ. 233, 111407 https://doi.org/10.1016/j.rse.2019.111407.
Wright, I.J., Reich, P.B., Westoby, M., Ackerly, D.D., Baruch, Z., Bongers, F., Villar, R., 2004. The worldwide leaf economics spectrum. Nature 428 (6985), 821–827. https://doi.org/10.1038/nature02403.
Zhang, J., Rivard, B., Sánchez-Azofeifa, A., Castro-Esau, K., 2006. Intra- and inter-class spectral variability of tropical tree species at La Selva, Costa Rica: implications for species identification using HYDICE imagery. Remote Sens. Environ. 105 (2), 129–141. https://doi.org/10.1016/j.rse.2006.06.010.